Model Reference Adaptive Control for Prescribed Performance and Longitudinal Control of a Tail-Sitter UAV

Julius A. Marshall *, Grant I. Carter †, and Andrea L'Afflitto ‡
Virginia Tech, Blacksburg, VA, 24061

Tail-sitter unmanned aerial vehicles (UAVs) merge the ability of multi-rotor aircraft, such as quadcopters, to take off, hover, and land vertically with the long endurance of fixed-wing aircraft. Therefore, tail-sitter UAVs can be employed in complex missions such as door-to-door payload delivery over extended regions. However, these vehicles' dynamics are nonlinear, and linear approximations poorly capture their behavior during the transition between vertical and horizontal flight regimes. Furthermore, these UAVs' aerodynamic coefficients are usually difficult to measure in all flight regimes. Therefore, designing controllers for tail-sitter UAVs is still an open problem. Model reference adaptive control (MRAC) for prescribed performance allows the user to impose *a priori* both bounds on the trajectory tracking error and the rate of convergence of the tracking error without modifying the reference model or employing estimators. In this paper, MRAC for prescribed performance is extended for the first time to pursue the output signal tracking problem despite matched and parametric uncertainties in the plant's dynamics. Successively, this adaptive control technique is applied to design a controller for the longitudinal dynamics of a class of tail-sitter UAVs, namely quad-biplanes, and enforce user-defined performance specifications despite modeling uncertainties in the vehicle's aerodynamic properties. Numerical simulations validate the applicability of the proposed control strategy and its advantages over classical MRAC.

Nomenclature

Γ, Γ_g	=	Adaptive rate matrices
$\alpha(\cdot)$	=	Angle of attack
$\theta(\cdot)$	=	Pitch angle
$\theta_{\rm cmd}(\cdot)$	=	Command pitch angle
$\gamma(\cdot)$	=	Flight path angle
$\varepsilon(\cdot)$	=	Auxiliary tracking error
$\lambda_{\max}(A)$, $\lambda_{\min}(A)$	=	Eigenvalues of $A \in \mathbb{R}^{n\times n}$ with maximum and minimum real parts, respectively
$\mathring{\mathcal{E}}$	=	Interior of $\mathcal{E} \subset \mathbb{R}^n$
$\mathrm{Re}(z)$	=	Real part of $z \in \mathbb{C}$
I_n	=	Identity matrix in $\mathbb{R}^{n\times n}$
$F_X^{\mathbb{I}}(\cdot)$, $F_Z^{\mathbb{I}}(\cdot)$	=	Components of the thrust force along the horizontal and vertical directions, respectively
$e(\cdot)$	=	Trajectory tracking error
$x_A(\cdot)$, $y_A(\cdot)$, $z_A(\cdot)$	=	UAV position in the inertial reference frame
$x_{A,\rm user}(\cdot)$, $z_{A,\rm user}(\cdot)$	=	User-defined reference trajectory
$x_{\rm p}(\cdot)$	=	Plant trajectory
$x_{\rm ref}(\cdot)$	=	Reference trajectory, deduced from $x_{A,\rm user}(\cdot)$, $z_{A,\rm user}(\cdot)$, and $\theta_{\rm cmd}(\cdot)$
$u(\cdot)$	=	Control input
0_n, $0_{n\times m}$	=	Zero vector in $\mathbb{R}^n$ and zero matrix in $\mathbb{R}^{n\times m}$, respectively
$\hat{(\cdot)}$	=	Estimated variable
$\tilde{(\cdot)}$	=	Augmented variable employed for output tracking
$(\cdot)_{\rm inner}$, $(\cdot)_{\rm outer}$	=	Variable employed in the inner or outer loops design, respectively

*Ph.D. Candidate, Grado Department of Industrial and Systems Engineering, AIAA student member.
†Graduate Student, Department of Mechanical Engineering.
‡Assistant Professor, Grado Department of Industrial and Systems Engineering, AIAA Senior Member.

I. Introduction

Tail-sitter unmanned aerial vehicles (UAVs) are equipped with multiple sets of propellers and wings and hence, are able to take off, hover, and land vertically like multi-rotor UAVs and fly horizontally over extended distances like fixed-wing UAVs. For these unique features, tail-sitters have the potential to merge the most relevant advantages of multi-rotor and fixed-wing airplanes without suffering from their major drawbacks. Indeed, multi-rotor UAVs, such as quadcopters, have proven their usefulness in multiple applications ranging from remote sensing to payload delivery. Among the key features that determined the success of multi-rotor UAVs, it is worthwhile recalling their ability to take off, hover, and land vertically and their relatively low fabrication and maintenance costs. However, multi-rotor UAVs usually suffer from a relatively short endurance, especially when transporting heavy payloads and performing missions that require large excursions in the vertical direction. To perform missions, in which long endurance is a fundamental prerequisite, fixed-wing UAVs are still a preferable option. However, fixed-wing UAVs are unable to hover. Moreover, these vehicles usually require either a runway or a launching mechanism to take off and a sufficiently long runway or a capture mechanism to land, which may not always be available.

Although tail-sitter aircraft were first patented in the US by Nikola Tesla in 1921 [1], this visionary configuration was developed only in 1951 for manned vehicles by Lockheed Martin with the XFV-1 aircraft and Convair with the XFY-1. These projects were suspended for the complexity of precisely controlling these aircraft, especially during the landing phase. More recently, the academic, defense, and industrial communities found new interest in tail-sitter UAVs [2–8]. However, tail-sitters are still challenging since their dynamics are nonlinear, and linear dynamical models, which underlie the overwhelming majority of commercial autopilots for multi-rotor and fixed-wing aircraft, poorly capture their behavior in the transition between the vertical and horizontal flight regimes. Additionally, these vehicles' aerodynamics is nonlinear and, although popular, aerodynamic models that are linear in the UAV's angle of attack are usually inaccurate, especially for maneuvers involving a rapid transition between the vertical and the horizontal regimes.

In this paper, we propose a control architecture to regulate the longitudinal dynamics of an autonomous quad-biplane UAV, that is, a tail-sitter aircraft equipped with two fixed wings and four propellers, whose spin axes are parallel to the UAV's roll axis; Figure 1 shows an image of a quad-biplane. Similarly to the vehicle considered in [8, 9], the quad-biplane considered in this paper is not equipped with any mobile surfaces, such as ailerons or elevators, and is controlled only by means of differential thrust, that is, by leveraging the difference in thrust produced by the propellers. This UAV's longitudinal dynamics are modeled assuming that the aerodynamic forces and moments are linear in the vehicle's angle of attack and, to maximize the applicability of the proposed control system, the UAV's wing surface area, its aerodynamic coefficients, and the air density are considered as unknown; remarkably, any aerodynamic model, which can be expressed as the product of an unknown constant matrix and a known linear or nonlinear vector function of time and the UAV's state, such as those employed in [10], can be employed in the proposed control architecture.

The proposed control architecture employs an inner and an outer loop. The outer loop computes both the norm of the thrust force and the orientation of the thrust force needed to follow a user-defined reference trajectory. The inner loop computes the moment of the thrust force needed to track the desired orientation of the thrust force. While computing the thrust force that each propeller needs to produce, multiple design criteria are considered. For instance, the propellers never point downward so that the aircraft can gain altitude as soon as required. Furthermore, the smallest thrust force to be produced by the propellers is user-defined since commercial-off-the-shelf components of small UAVs do not allow to produce arbitrarily small thrust. Worthy of mention is that in this paper, we account for the aerodynamic forces and moments acting on the UAV irrespectively of the UAV's flight path angle; similar modeling assumptions have been employed in [9, 11]. This modeling decision allows the autopilot to better control the UAV over the course of maneuvers and exploit both the lift force and the propellers' thrust force for climbing or descending at high pitch angles.

The controller's inner and outer loops comprise both a baseline controller, which attempts a feedback linearization of the UAV's dynamics, and an adaptive controller, which compensates for modeling uncertainties and errors in linearizing the aircraft dynamics. This adaptive controller is designed by applying four alternative model reference adaptive control (MRAC) laws, namely a classical MRAC law for state tracking [12, Ch. 9], a classical MRAC law for output signal tracking [12, Ch. 10], a MRAC law for prescribed performance and state tracking [13], and an original MRAC law for prescribed performance and output signal tracking. The MRAC laws for prescribed performance allow to impose both a user-defined rate of convergence and user-defined bounds on the tracking error. This result is achieved while setting the adaptive rates arbitrarily and without introducing estimators or differentiators, and without modifying the reference model. Alternative techniques attain similar results through a careful tuning of the adaptive rates [14–18], involve estimators or differentiators [19–22], or require modifying the reference model by introducing an error feedback term [23–25].

To the authors' knowledge, this is the first paper to present an MRAC control architecture to regulate the longitudinal

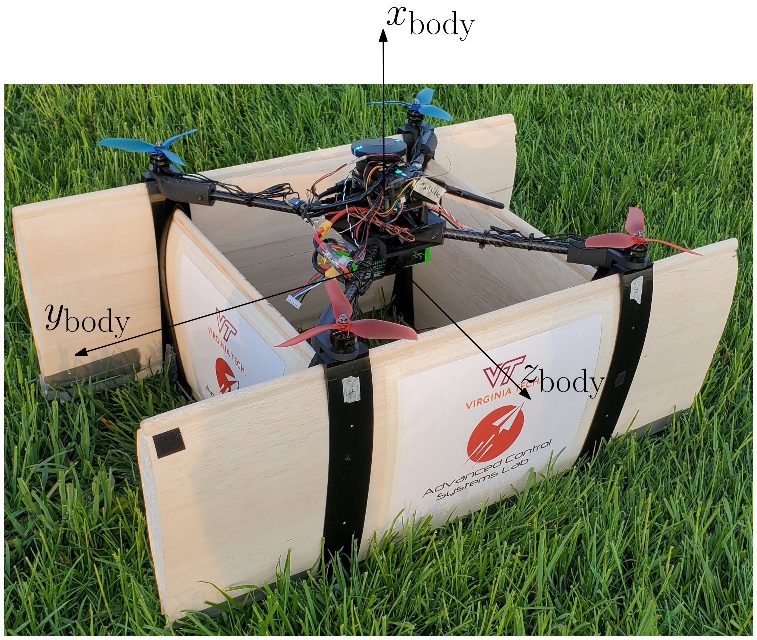

Fig. 1 Quad-biplane UAV designed and fabricated at the Advanced Control Systems Lab at Virginia Tech.

dynamics of a tail-sitter UAV. Furthermore, MRAC for prescribed performance is still a new control technique. The problem of controlling tail-sitter UAVs has been addressed by applying the classical proportional-integral-derivative control law [4, 26–29], the linear-quadratic regulator [30] and other optimal control-based techniques [31], gain scheduling [32], backstepping [33], and $\mathcal{L}_1$ adaptive control [34] to name a few of the most popular linear and nonlinear control techniques. However, none of these approaches is able to impose *a priori* user-defined constraints and a user-defined rate of convergence on the closed-loop tracking error. To our knowledge, the only work involving a tailsitter UAV and an MRAC law is presented in [35], where the classical direct MRAC law is applied to control exclusively the pitch dynamics of a tail-sitter UAV, while the problem of controlling translational dynamics in the longitudinal plane is not addressed. It is worthwhile to remark that the proposed architecture allows the user to outline the UAV's reference trajectory arbitrarily. In several cases, the tail-sitter's controller is provided with the desired orientation and altitude, while the UAV's position in the horizontal plane is deduced applying an open-loop mechanism [11, 36–38].

This paper is structured as follows. In Section II, we recall fundamental elements of MRAC theory. In Section III, we present the MRAC for prescribed performance architecture and extend it to output signal tracking. In Section IV, we present a dynamical model for the longitudinal dynamics of a tail-sitter UAV, verify the under-actuation of these vehicles, and propose an inner and outer loop control architecture. In Section V, we present the outcomes of numerical simulations aimed at showing the efficacy of both MRAC for prescribed performance and the proposed control architecture for tail-sitters. Finally, in Section VI, we draw conclusions and outline future work directions.

II. Fundamentals of Model Reference Adaptive Control Theory

A. Classical MRAC for state tracking

In this section, we recall fundamental results from classical MRAC framework. To this goal, consider the nonlinear *plant dynamics*

$$\dot{x}_{\mathrm{p}}(t) = A_{\mathrm{p}}x_{\mathrm{p}}(t) + B_{\mathrm{p}}\left[u(t) + \Theta^{\mathrm{T}}\Phi(t, x_{\mathrm{p}}(t))\right], \qquad x_{\mathrm{p}}(t_0) = x_{\mathrm{p},0}, \qquad t \geq t_0, \tag{1}$$

$$y(t) = C_{\mathrm{p}}x_{\mathrm{p}}(t) + D_{\mathrm{p}}\left[u(t) + \Theta^{\mathrm{T}}\Phi(t, x_{\mathrm{p}}(t))\right], \tag{2}$$

where $x_{\mathrm{p}}(t) \in \mathcal{D} \subseteq \mathbb{R}^n$, $t \geq t_0 \geq 0$, denotes the *plant trajectory*, $0 \in \mathcal{D}$, $u(t) \in \mathbb{R}^m$ denotes the *control input*, $y(t) \in \mathbb{R}^m$ denotes the *plant measured output*, $A_{\mathrm{p}} \in \mathbb{R}^{n\times n}$ is unknown, $B_{\mathrm{p}} \in \mathbb{R}^{n\times m}$ is known, $C_{\mathrm{p}} \in \mathbb{R}^{m\times n}$ is known, $D_{\mathrm{p}} \in \mathbb{R}^{m\times m}$ is known, the pair $(A_{\mathrm{p}}, B_{\mathrm{p}})$ is controllable, $\Theta \in \mathbb{R}^{N\times m}$ is unknown, the user-defined *regressor vector*

$\Phi : [t_0, \infty) \times \mathcal{D} \to \mathbb{R}^N$ is jointly continuous in its arguments, $\Phi(\cdot, x_{\rm p})$ is bounded in t over $[t_0, \infty)$, and $\Phi(t, \cdot)$ is locally Lipschitz continuous in $x_{\rm p}$ uniformly in t on compact subsets of $[t_0, \infty)$. The matrix $A_{\rm p}$ captures *parametric uncertainties*, and $\Theta^{\rm T}\Phi(t, x_{\rm p})$, $(t, x_{\rm p}) \in [t_0, \infty) \times \mathcal{D}$, captures *matched uncertainties*; the choice of the regressor vector $\Phi(\cdot, \cdot)$ to parameterize uncertainties is usually based on some prior knowledge of the plant dynamics [12, Ch. 9]. In numerous problems of practical interest, the structure of $A_{\rm p}$ is known, and it is possible to verify the controllability of the pair $(A_{\rm p}, B_{\rm p})$. Consider also the *plant's reference model*

$$\dot{x}_{\rm ref}(t) = A_{\rm ref}x_{\rm ref}(t) + B_{\rm ref}r(t), \qquad x_{\rm ref}(t_0) = x_{\rm ref,0}, \qquad t \geq t_0, \tag{3}$$

$$y_{\rm ref}(t) = C_{\rm ref}x_{\rm ref}(t), \tag{4}$$

where $x_{\rm ref}(t) \in \mathbb{R}^n$, $t \geq t_0$, denotes the *reference trajectory*, the *reference command input* $r(t) \in \mathbb{R}^m$ is continuous and bounded, $y_{\rm ref}(t) \in \mathbb{R}^m$, denotes the *reference measured output*, $A_{\rm ref} \in \mathbb{R}^{n\times n}$ is Hurwitz, $B_{\rm ref} \in \mathbb{R}^{n\times m}$, $C_{\rm ref} \in \mathbb{R}^{m\times n}$, and assume there exist $(K_x, K_r) \in \mathbb{R}^{n\times m} \times \mathbb{R}^{m\times m}$ such that the *matching conditions*

$$A_{\rm ref} = A_{\rm p} + B_{\rm p}K_x^{\rm T}, \tag{5}$$

$$B_{\rm ref} = B_{\rm p}K_r^{\rm T}, \tag{6}$$

are verified. Since $A_{\rm ref}$, $B_{\rm p}$, and $B_{\rm ref}$ are known and, in numerous problems of practical interest, the structure of $A_{\rm p}$ is known, it is possible to prove the existence of K_x and K_r that verify the matching conditions (5) and (6), respectively [12, p. 282]. Finally, let $e(t) \triangleq x_{\rm p}(t) - x_{\rm ref}(t)$ denote the *trajectory tracking error*.

The next result illustrates the classical MRAC architecture. For the statement of this result define the *feedback control law*

$$\phi_{\rm MRAC}(\pi(t, x_{\rm p}, r), \hat{K}) \triangleq \hat{K}^{\rm T}\pi(t, x_{\rm p}, r), \qquad (t, x_{\rm p}, r, \hat{K}) \in [t_0, \infty) \times \mathcal{D} \times \mathbb{R}^m \times \mathbb{R}^{(n+m+N)\times m}, \tag{7}$$

where the *adaptive gain matrix* $\hat{K}(\cdot)$ verifies the *adaptive law*

$$\dot{\hat{K}}(t) = -\Gamma\pi(t, x_{\rm p}(t), r(t))e^{\rm T}(t)PB, \qquad \hat{K}(t_0) = \hat{K}_0, \qquad t \geq t_0, \tag{8}$$

$\Gamma \triangleq \text{blockdiag}\,(\Gamma_x, \Gamma_r, \Gamma_\Theta)$, the user-defined *adaptive rate matrices* $\Gamma_x \in \mathbb{R}^{n\times n}$, $\Gamma_r \in \mathbb{R}^{m\times m}$, and $\Gamma_\Theta \in \mathbb{R}^{N\times N}$ are symmetric and positive-definite, $P \in \mathbb{R}^{n\times n}$ denotes the symmetric positive-definite solution of the *algebraic Lyapunov equation*

$$0 = A_{\rm ref}^{\rm T}P + PA_{\rm ref} + Q, \tag{9}$$

$Q \in \mathbb{R}^{n\times n}$ denotes a user-defined symmetric positive-definite matrix, and

$$\pi(t, x_{\rm p}, r) \triangleq \left[x_{\rm p}^{\rm T}, r^{\rm T}, -\Phi^{\rm T}(t, x_{\rm p})\right]^{\rm T} \tag{10}$$

denotes the *vector of feedback variables*.

Theorem II.1 ([12, Th. 9.2]) *Consider the plant's dynamics* (1)*, the plant's reference model* (3)*, the feedback control law* (7)*, and the adaptive law* (8)*. If the matching conditions* (5) *and* (6) *are verified and* $u(t) = \phi_{\rm MRAC}(\pi(t, x_{\rm p}(t), r(t)), \hat{K}(t))$*,* $t \geq t_0$*, then both the trajectory tracking error* $e(\cdot)$ *and the adaptive gain matrix* $\hat{K}(\cdot)$ *are uniformly bounded, and* $e(t) \to 0$ *as* $t \to \infty$ *uniformly in* $t_0 \in [0, \infty)$.

B. MRAC for output signal tracking

The next result leverages the classical MRAC architecture and allows the plant measured output $y(\cdot)$ to follow a user-defined bounded *reference signal* $y_{\rm cmd} : [t_0, \infty) \to \mathbb{R}^m$ with bounded error. For the statement of this result, assume that $A_{\rm p}$ is known and $D_{\rm p} \neq 0_{m\times m}$. Additionally, define $\tilde{A} \triangleq \begin{bmatrix} 0_{m\times m} & C_{\rm p} \\ 0_{n\times m} & A_{\rm p} \end{bmatrix}$, $\tilde{B} \triangleq \begin{bmatrix} D_{\rm p} \\ B_{\rm p} \end{bmatrix}$, $\tilde{C} \triangleq \left[0_{m\times m}, C_{\rm p}\right]$, and let $P_{\rm LQR} \in \mathbb{R}^{(n+m)\times(n+m)}$ denote the symmetric positive-definite solution of the *algebraic Riccati equation*

$$0 = \tilde{A}^{\rm T}P_{\rm LQR} + P_{\rm LQR}\tilde{A} + Q_{\rm LQR} - P_{\rm LQR}\tilde{B}R^{-1}\tilde{B}^{\rm T}P_{\rm LQR}, \tag{11}$$

where $R \in \mathbb{R}^{m\times m}$ and $Q_{\rm LQR} \in \mathbb{R}^{(n+m)\times(n+m)}$ are user-defined, symmetric, and positive-definite. Furthermore, let $e_{y,{\rm I}}(t) \triangleq \int_{t_0}^{t}[y(\tau) - y_{\rm cmd}(\tau)]{\rm d}\tau$, $t \geq t_0$, denote the *integral output tracking error*, let

$$x(t) \triangleq \left[e_{y,{\rm I}}^{\rm T}(t), x_{\rm p}^{\rm T}(t)\right]^{\rm T} \tag{12}$$

denote the *augmented state vector*, define $\tilde{A}_{\rm ref} \triangleq \tilde{A}-\tilde{B}R^{-1}\tilde{B}^{\rm T}P_{\rm LQR}$, $\tilde{B}_{\rm ref} \triangleq [-I_m, 0_{m\times n}]^{\rm T}$, and $\tilde{C}_{\rm ref} \triangleq \tilde{C}-D_{\rm p}R^{-1}\tilde{B}^{\rm T}P_{\rm LQR}$, let $\tilde{x}_{\rm ref}(\cdot)$ denote the solution of

$$\dot{\tilde{x}}_{\rm ref}(t) = \tilde{A}_{\rm ref}\tilde{x}_{\rm ref}(t) + \tilde{B}_{\rm ref}y_{\rm cmd}(t), \qquad \tilde{x}_{\rm ref}(t_0) = \left[0_m^{\rm T}, x_{{\rm ref},0}^{\rm T}\right]^{\rm T}, \qquad t \geq t_0, \tag{13}$$

and define the *augmented trajectory tracking error* $\tilde{e}(t) \triangleq x(t) - \tilde{x}_{\rm ref}(t)$. Finally, define the feedback control law

$$\phi_{\rm MRAC,tracking}(\pi_{\rm tracking}(t,x), \tilde{K}) \triangleq -R^{-1}\tilde{B}^{\rm T}P_{\rm LQR}x + \tilde{K}^{\rm T}\pi_{\rm tracking}(t,x), \quad (t,x,\tilde{K}) \in [t_0,\infty)\times\mathbb{R}^{n+m}\times\mathbb{R}^{(n+m+N)\times m}, \tag{14}$$

where

$$\pi_{\rm tracking}(t,x) \triangleq \left[-\left(R^{-1}\tilde{B}^{\rm T}P_{\rm LQR}x\right)^{\rm T}, \Phi^{\rm T}(t,x_{\rm p})\right]^{\rm T} \tag{15}$$

denotes the *vector of feedback variables*,

$$\dot{\tilde{K}}(t) = \tilde{\Gamma}\pi_{\rm tracking}(t,x(t))\tilde{e}^{\rm T}(t)P_y\tilde{B}, \qquad \tilde{K}(t_0) = \tilde{K}_0, \qquad t \geq t_0, \tag{16}$$

$\tilde{\Gamma} \triangleq$ blockdiag $(\Gamma_{\rm LQR}, \Gamma_\Theta)$, the user-defined adaptive rate matrices $\Gamma_{\rm LQR} \in \mathbb{R}^{(n+m)\times(n+m)}$ and $\Gamma_\Theta \in \mathbb{R}^{N\times N}$ are symmetric and positive-definite, $P_y \in \mathbb{R}^{(n+m)\times(n+m)}$ denotes the symmetric, positive-definite solution of the algebraic Lyapunov equation

$$0 = \tilde{A}_{\rm ref}^{\rm T}P_y + P_y\tilde{A}_{\rm ref} + Q_y, \tag{17}$$

and $Q_y \in \mathbb{R}^{(n+m)\times(n+m)}$ is symmetric, positive-definite, and user-defined.

Theorem II.2 ([12, pp. 303-310]) *Consider the plant's dynamical model* (1) *and* (2)*, the bounded reference signal* $y_{\rm cmd}(\cdot)$*, the feedback control law* (14)*, and the adaptive law* (16)*. If* $A_{\rm p}$ *is known,* $D_{\rm p} \neq 0_{m\times m}$*, and* $u(t) = \phi_{\rm MRAC,tracking}(\pi_{\rm tracking}(t,x(t)), \tilde{K}(t))$*,* $t \geq t_0$*, then both the plant trajectory* $x_{\rm p}(\cdot)$ *and the adaptive gain matrix* $\tilde{K}(\cdot)$ *are uniformly bounded, and* $\|y(t) - C_{\rm p}x_{\rm p}(t)\| \to 0$ *and* $\|y(t) - \tilde{C}_{\rm ref}\tilde{x}_{\rm ref}(t)\| \to 0$ *as* $t \to \infty$ *uniformly in* $t_0 \in [0,\infty)$*. Furthermore,* $\|y(t) - y_{\rm cmd}(t)\|$*,* $t \geq t_0$*, is uniformly bounded.*

In practical applications, if $y_{\rm cmd}(\cdot)$ varies sufficiently slowly, then, by applying the control law (14) and the adaptive law (16), the plant measured output $y(\cdot)$ converges to the reference signal $y_{\rm cmd}(\cdot)$. In order to apply Theorem II.2, it must hold that $D_{\rm p} \neq 0_{m\times m}$; this condition is needed to guarantee that the Hamiltonian matrix underlying the Riccati equation (11) does not have eigenvalues on the imaginary axis. However, the result whereby $\lim_{t\to\infty}\|y(t) - C_{\rm p}x_{\rm p}(t)\| = 0$ uniformly in $t_0 \in [0,\infty)$ compensates for this technical requirement. Lastly, the result whereby $\lim_{t\to\infty}\|y(t) - \tilde{C}_{\rm ref}\tilde{x}_{\rm ref}(t)\| = 0$ uniformly in $t_0 \in [0,\infty)$ implies that the plant measured output $y(\cdot)$ tracks

$$\tilde{y}_{\rm ref}(t) \triangleq \tilde{C}\tilde{x}_{\rm ref}(t) - D_{\rm p}u_{\rm baseline}(t), \qquad t \geq t_0,$$

where $u_{\rm baseline}(t) \triangleq -R^{-1}\tilde{B}^{\rm T}P_{\rm LQR}\tilde{x}_{\rm ref}(t)$ denotes the *baseline controller*.

III. Model Reference Adaptive Control for Prescribed Performance

A. Motivation

In this section, we recall the MRAC for prescribed performance architecture, which has been recently devised by the authors in [13]. This architecture allows to overcome two main limitations of the classical MRAC framework presented by Theorem II.1. To discuss the first of these limitations, it is worthwhile recalling the notion of rate of convergence of a linear, asymptotically stable dynamical system with bounded control input.

Definition III.1 *Consider the linear, time-invariant, asymptotically stable dynamical system with bounded input* (3). *The rate of convergence of* $x_{\rm ref}(\cdot)$ *is defined as*

$$\alpha_{\max}(x_{\rm ref}(\cdot)) \triangleq \sup_{x_{\rm ref,0}\in\mathbb{R}^n\setminus\{0\}} \liminf_{t\to\infty} \frac{\log\|x_{\rm ref}(t)\|}{t_0 - t}. \tag{18}$$

It follows from (1), (3), and (5)–(7) that the trajectory tracking error dynamics is given by

$$\dot{e}(t) = A_{\rm ref}e(t) + B_{\rm p}\left[\hat{K}(t) - K\right]^{\rm T}\pi(t, x_{\rm p}(t), r(t)), \qquad e(t_0) = x_{\rm p,0} - x_{\rm ref,0}, \qquad t \geq t_0, \tag{19}$$

where $K \triangleq [K_x, K_r, \Theta]$. Thus, as proven in [12, Ch. 13] and [13], both the trajectory tracking error dynamics (19) and the reference model's dynamics (3) are characterized by the same rate of convergence, that is, $\alpha_{\max}(e(\cdot)) = -{\rm Re}(\lambda_{\max}(A_{\rm ref}))$ and $\alpha_{\max}(x_{\rm ref}(\cdot)) = -{\rm Re}(\lambda_{\max}(A_{\rm ref}))$. Therefore, in general, the closed-loop plant trajectory $x_{\rm p}(\cdot)$ reaches the reference trajectory $x_{\rm ref}(\cdot)$ as soon as or after the transient dynamics of reference model has decayed. However, this is a limitation of the classical MRAC architecture since it would be desirable to design an MRAC law so that

$$\alpha_{\max}\left(e(\cdot)\right) \geq \alpha, \tag{20}$$

where $\alpha > -{\rm Re}(\lambda_{\min}(A_{\rm ref})) \geq -{\rm Re}(\lambda_{\max}(A_{\rm ref}))$ is a user-defined parameter [12, pp. 389-390]. MRAC for prescribed performance meets this requirement, that is, it allows to impose *a priori* the rate of convergence of the closed-loop trajectory tracking error, while setting the adaptive rates arbitrarily large, without involving estimators or differentiators, and without modifying the reference model by means of an error feedback term.

Classical MRAC is also unable to directly impose user-defined bounds on the norm of the tracking error $\|e(\cdot)\|$; these bounds can only be either estimated *a priori* in a conservative manner or verified *a posteriori*. MRAC for prescribed performance allows to impose *a priori* arbitrary bounds on the trajectory tracking error.

B. MRAC for prescribed performance and state tracking

To present MRAC for prescribed performance, consider the plant (1), the plant's reference model (3), and the *constraint set*

$$\mathcal{E} \triangleq \left\{e \in \mathbb{R}^n : h_e(e^{\rm T}Me) \geq 0\right\}, \tag{21}$$

where $M \in \mathbb{R}^{n\times n}$ denotes a symmetric and positive-definite solution of the linear matrix inequality

$$A_{\rm ref}^{\rm T}M + MA_{\rm ref} \leq 0, \tag{22}$$

$h_e : \mathbb{R} \to \mathbb{R}$, $h_e(0) > 0$, and $h_e(\cdot)$ is continuously differentiable for all $e \in \mathcal{E}$. Furthermore, consider the feedback control law

$$\begin{aligned}\phi(\pi(t, x_{\rm p}, r), e, \hat{K}, \hat{K}_g) &= \hat{K}^{\rm T}\pi(t, x_{\rm p}, r) + \hat{K}_g^{\rm T}e,\\ &(t, x_{\rm p}, e, r, \hat{K}, \hat{K}_g) \in [t_0, \infty) \times \mathcal{D} \times \mathbb{R}^n \times \mathbb{R}^m \times \mathbb{R}^{(n+m+N)\times m} \times \mathbb{R}^{n\times m},\end{aligned} \tag{23}$$

where the vector of feedback variables $\pi(\cdot,\cdot,\cdot)$ is given by (10), and define $h'_e : \mathbb{R} \to \mathbb{R}$ such that

$$h'_e(e^{\rm T}Me) \triangleq \left.\frac{\partial h_e(\beta)}{\partial\beta}\right|_{\beta = e^{\rm T}Me}, \qquad e \in \mathbb{R}^n. \tag{24}$$

Additionally, let

$$V_e(e, \varepsilon) \triangleq h_e^{-1}(e^{\rm T}Me)\varepsilon^{\rm T}P_{\rm transient}\varepsilon, \qquad (e, \varepsilon) \in \mathring{\mathcal{E}} \times \mathbb{R}^n, \tag{25}$$

$$V_g(\hat{K}_g) \triangleq {\rm tr}^{\frac{1}{2}}\left(\Delta K_g^{\rm T}\Gamma_g^{-1}\Delta K_g\right), \qquad \hat{K}_g \in \mathbb{R}^{n\times m}, \tag{26}$$

where $\Gamma_g \in \mathbb{R}^{n\times n}$ denotes a user-defined, symmetric, and positive-definite *adaptive rate matrix*, $\Delta K_g(t) \triangleq \hat{K}_g(t) - K_e$, $K_e \in \mathbb{R}^{n\times m}$ verifies the matching condition

$$A_{\rm transient} = A_{\rm ref} + BK_e^{\rm T}, \tag{27}$$

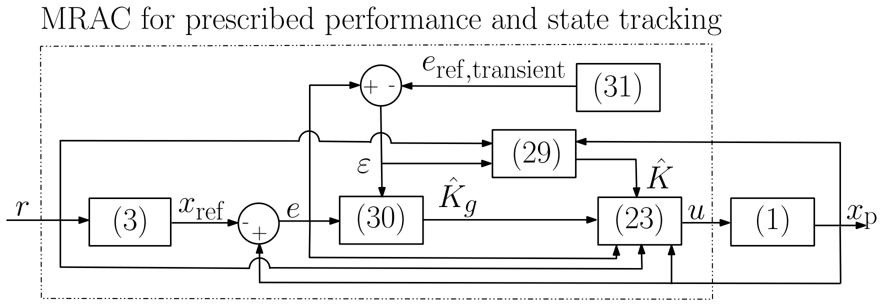

Fig. 2 Graphical representation of the MRAC for prescribed performance architecture presented in Theorem III.1. Applying the control law (23) **and the adaptive laws** (29) **and** (30)**, Theorem III.1 guarantees uniform boundedness of both the closed-loop system's trajectory error** $e(\cdot)$ **and the adaptive gain matrices** $\hat{K}(\cdot)$ **and** $\hat{K}_g(\cdot)$**. Moreover, Theorem III.1 guarantees uniform asymptotic convergence of** $e(\cdot)$ **to zero. Lastly, Theorem III.1 guarantees that** $x_{\text{p}}(\cdot)$ **reaches** $x_{\text{ref}}(\cdot)$ **before the transient dynamics of the plant's reference model** (3) **has decayed.**

$A_{\text{transient}} \in \mathbb{R}^{n\times n}$ is user-defined and Hurwitz, $P_{\text{transient}} \in \mathbb{R}^{n\times n}$ denotes the symmetric, positive-definite solution of the algebraic Lyapunov equation

$$0 = A_{\text{transient}}^{\text{T}} P_{\text{transient}} + P_{\text{transient}} A_{\text{transient}} + Q_{\text{transient}}, \tag{28}$$

and $Q_{\text{transient}} \in \mathbb{R}^{n\times n}$ is user-defined, symmetric, and positive-definite. Finally, consider the adaptive laws

$$\dot{\hat{K}}(t) = -\Gamma \frac{\pi(t, x_{\text{p}}(t), r(t))}{h_e(e^{\text{T}}(t)Me(t))} \varepsilon^{\text{T}}(t) \Big[P_{\text{transient}} - V_e(e(t),\varepsilon(t)) h_e'(e^{\text{T}}(t)Me(t))M \Big] B, \qquad \hat{K}(t_0) = \hat{K}_0, \qquad t \geq t_0, \tag{29}$$

$$\dot{\hat{K}}_g(t) = -\frac{2V_g(\hat{K}_g(t))}{h_e(e^{\text{T}}(t)Me(t))} \Gamma_g e(t)\varepsilon^{\text{T}}(t) \left[P_{\text{transient}} - V_e(e(t),\varepsilon(t)) h_e'(e^{\text{T}}(t)Me(t))M \right] B, \qquad \hat{K}_g(t_0) = \hat{K}_{g,0}, \tag{30}$$

where $\hat{K}_g(t_0) \neq K_e$ and $\hat{K}_g(t_0) \neq 0$, $\Gamma \in \mathbb{R}^{(n+m+N)\times(n+m+N)}$ denotes a user-defined symmetric and positive-definite *adaptive rate matrix*, $\varepsilon(t) \triangleq e(t) - e_{\text{ref,transient}}(t)$ denotes the *auxiliary tracking error*, and $e_{\text{ref,transient}}(\cdot)$ denotes the solution of

$$\dot{e}_{\text{ref,transient}}(t) = A_{\text{transient}} e_{\text{ref,transient}}(t), \qquad e_{\text{ref,transient}}(t_0) = x_{\text{p}}(t_0) - x_{\text{ref}}(t_0). \tag{31}$$

The next result illustrates the MRAC for prescribed performance architecture, which is graphically illustrated in Figure 2.

Theorem III.1 *Consider the plant's dynamics* (1)*, the plant's reference model* (3)*, the constraint set* (21)*, the feedback control law* (23)*, and the adaptive laws* (29) *and* (30)*. If* $e(t_0) \in \mathring{\mathcal{E}}$*,* $h_e'(e^{\text{T}}Me) \leq 0$ *for all* $e \in \mathring{\mathcal{E}}$*, the matching conditions* (5)*,* (6)*, and* (27) *are verified, and* $\text{Re}(\lambda_{\max}(A_{\text{transient}})) < \text{Re}(\lambda_{\min}(A_{\text{ref}}))$*, then both the trajectory tracking error* $e(\cdot)$ *and the adaptive gain matrices* $\hat{K}(\cdot)$ *and* $\hat{K}_g(\cdot)$ *are uniformly bounded. Moreover,* $e(t) \in \mathring{\mathcal{E}}$*,* $t \geq t_0$*, and* $e(t) \to 0$ *and* $\varepsilon(t) \to 0$ *as* $t \to \infty$ *uniformly in* $t_0 \in [0,\infty)$*. Lastly,* (20) *is verified with* $\alpha > -\text{Re}(\lambda_{\min}(A_{\text{ref}})) \geq -\text{Re}(\lambda_{\max}(A_{\text{ref}}))$*.*

Proof: The result follows as a direct consequence of Theorem 6.2 of [13]. ■

Theorem III.1 guarantees uniform asymptotic convergence of the closed-loop system's trajectory tracking error, uniform boundedness of the trajectory tracking error $e(\cdot)$ and of the adaptive gains $\hat{K}(\cdot)$ and $\hat{K}_g(\cdot)$, and verification of the user-defined constraints captured by (21). Furthermore, Theorem III.1 allows the user to impose a rate of convergence on the trajectory tracking error by choosing $A_{\text{transient}}$. This result has been attained by exploiting the barrier Lyapunov function (25) to enforce user-defined constraints captured by the set $\mathcal{E}$ and by steering the closed-loop plant trajectory toward an auxiliary reference model, whose state converges to $x_{\text{ref}}(\cdot)$ with a rate that is faster than the rate of convergence of (3). The closed ball of radius $\kappa > 0$ centered at zero, which is captured by

$$\mathcal{E} = \{e \in \mathbb{R}^n : \kappa^2 - e^{\text{T}}e \geq 0\},$$

provides an example of constraint set such that (22) is verified with $M = I_n$ and the condition $h_e'(e^{\text{T}}Me) < 0$ in Theorem III.1 is verified for all $e \in \mathring{\mathcal{E}}$. For additional details on the MRAC for prescribed performance architecture, detailed proofs, and comparisons with alternative techniques such as classical prescribed performance control [39, 40], see [13].

C. MRAC for prescribed performance and output signal tracking

Similarly to Theorem II.1, Theorem III.1 provides a control law and adaptive laws such that the closed-loop plant trajectory $x_{\mathrm{p}}(\cdot)$ follows the reference trajectory $x_{\mathrm{ref}}(\cdot)$. The next result leverages Theorem III.1 and provides a control law and adaptive laws such that the closed-loop plant measured output $y(\cdot)$ tracks a user-defined bounded reference signal $y_{\mathrm{cmd}}(\cdot)$. For the statement of this result, assume that A_{p} is known and $D_{\mathrm{p}} \neq 0_{m\times m}$. Additionally, let

$$\tilde{\mathcal{E}} \triangleq \left\{\tilde{e} \in \mathbb{R}^{n+m} : h_e(\tilde{e}^{\mathrm{T}}\tilde{M}\tilde{e}) \geq 0\right\}, \tag{32}$$

denote a constraint set for the augmented trajectory tracking error vector $\tilde{e}(\cdot)$, where $\tilde{M} \in \mathbb{R}^{(n+m)\times(n+m)}$ is a symmetric and positive-definite solution of the inequality

$$\tilde{A}_{\mathrm{ref}}^{\mathrm{T}}\tilde{M} + \tilde{M}\tilde{A}_{\mathrm{ref}} \leq 0; \tag{33}$$

it is worthwhile to note that $\tilde{\mathcal{E}}$ captures constraints both on the trajectory tracking error $e(\cdot)$ and the integral output tracking error $e_{y,\mathrm{I}}(\cdot)$. Define also

$$\tilde{V}_e(\tilde{e},\tilde{\varepsilon}) \triangleq h_e^{-1}(\tilde{e}^{\mathrm{T}}\tilde{M}\tilde{e})\tilde{\varepsilon}^{\mathrm{T}}\tilde{P}_{\mathrm{transient}}\tilde{\varepsilon}, \qquad (\tilde{e},\tilde{\varepsilon}) \in \mathring{\tilde{\mathcal{E}}} \times \mathbb{R}^{n+m}, \tag{34}$$

$$\tilde{V}_g(\hat{K}_g) \triangleq \mathrm{tr}^{\frac{1}{2}}\left(\Delta\tilde{K}_g^{\mathrm{T}}\tilde{\Gamma}_g^{-1}\Delta\tilde{K}_g\right), \qquad \tilde{K}_g \in \mathbb{R}^{(n+m)\times m}, \tag{35}$$

where $\tilde{\Gamma}_g \in \mathbb{R}^{(n+m)\times(n+m)}$ denotes a user-defined symmetric and positive-definite *adaptive rate matrix*, $\Delta\tilde{K}_g(t) \triangleq \tilde{K}_g(t) - \tilde{K}_e$, $\tilde{K}_e \in \mathbb{R}^{(n+m)\times m}$ verifies the matching condition

$$\tilde{A}_{\mathrm{transient}} = \tilde{A}_{\mathrm{ref}} + \tilde{B}\tilde{K}_e^{\mathrm{T}}, \tag{36}$$

$\tilde{A}_{\mathrm{transient}} \in \mathbb{R}^{(n+m)\times(n+m)}$ is user-defined and Hurwitz, $\tilde{P}_{\mathrm{transient}} \in \mathbb{R}^{(n+m)\times(n+m)}$ denotes the symmetric, positive-definite solution of the algebraic Lyapunov equation

$$0 = \tilde{A}_{\mathrm{transient}}^{\mathrm{T}}\tilde{P}_{\mathrm{transient}} + \tilde{P}_{\mathrm{transient}}\tilde{A}_{\mathrm{transient}} + \tilde{Q}_{\mathrm{transient}}, \tag{37}$$

and $\tilde{Q}_{\mathrm{transient}} \in \mathbb{R}^{(n+m)\times(n+m)}$ is user-defined, symmetric, and positive-definite. Finally, define the feedback control law

$$\begin{aligned}\phi_{\mathrm{tracking}}(\pi_{\mathrm{tracking}}(t,x), e, \tilde{K}, \hat{K}_g) &\triangleq -R^{-1}\tilde{B}^{\mathrm{T}}P_{\mathrm{LQR}}x + \tilde{K}^{\mathrm{T}}\pi_{\mathrm{tracking}}(t,x) + \hat{K}_g^{\mathrm{T}}\tilde{e},\\ &(t,x,e,\tilde{K},\hat{K}_g) \in [t_0,\infty)\times\mathbb{R}^{n+m}\times\mathbb{R}^{n+m}\times\mathbb{R}^{(n+m+N)\times m}\times\mathbb{R}^{(n+m)\times m},\end{aligned} \tag{38}$$

where

$$\dot{\tilde{K}}(t) = \frac{\tilde{\Gamma}\pi_{\mathrm{tracking}}(t,x(t))\tilde{\varepsilon}^{\mathrm{T}}(t)}{h_e(\tilde{e}^{\mathrm{T}}(t)\tilde{M}\tilde{e}(t))}\left[\tilde{P}_{\mathrm{transient}} - \tilde{V}_e(\tilde{e}(t),\tilde{\varepsilon}(t))h_e'(\tilde{e}^{\mathrm{T}}(t)\tilde{M}\tilde{e}(t))\tilde{M}\right]\tilde{B}, \qquad \tilde{K}(t_0) = \tilde{K}_0, \qquad t \geq t_0, \tag{39}$$

$$\dot{\hat{K}}_g(t) = -\frac{2\tilde{V}_g(\hat{K}_g(t))}{h_e(\tilde{e}^{\mathrm{T}}(t)\tilde{M}\tilde{e}(t))}\tilde{\Gamma}_g\tilde{e}(t)\tilde{\varepsilon}^{\mathrm{T}}(t)\left[\tilde{P}_{\mathrm{transient}} - \tilde{V}_e(\tilde{e}(t),\tilde{\varepsilon}(t))h_e'(\tilde{e}^{\mathrm{T}}(t)\tilde{M}\tilde{e}(t))\tilde{M}\right]\tilde{B}, \qquad \hat{K}_g(t_0) = \hat{K}_{g,0}, \tag{40}$$

$\hat{K}_g(t_0) \neq \tilde{K}_e$ and $\hat{K}_g(t_0) \neq 0$, $\tilde{\varepsilon}(t) \triangleq \tilde{e}(t) - \tilde{e}_{\mathrm{ref,transient}}(t)$ denotes the *auxiliary tracking error*, $\tilde{e}_{\mathrm{ref,transient}}(\cdot)$ denotes the solution of

$$\dot{\tilde{e}}_{\mathrm{ref,transient}}(t) = \tilde{A}_{\mathrm{transient}}\tilde{e}_{\mathrm{ref,transient}}(t), \qquad \tilde{e}_{\mathrm{ref,transient}}(t_0) = x(t_0) - \tilde{x}_{\mathrm{ref}}(t_0). \tag{41}$$

and $\tilde{\Gamma}_g \in \mathbb{R}^{(n+m)\times(n+m)}$ denotes a user-defined, symmetric, and positive-definite *adaptive rate matrix*.

Theorem III.2 *Consider the plant's dynamics* (1) *and* (2)*, the reference model* (13)*, the constraint set* (32)*, the feedback control law* (38)*, and the adaptive laws* (39) *and* (40)*. If* $\tilde{e}(t_0) \in \mathring{\tilde{\mathcal{E}}}$*,* $h_e'(\tilde{e}^{\mathrm{T}}\tilde{M}\tilde{e}) \leq 0$ *for all* $\tilde{e} \in \mathring{\tilde{\mathcal{E}}}$*,* A_{p} *is known,* $D_{\mathrm{p}} \neq 0_{m\times m}$*, the matching condition* (36) *is verified,* $\mathrm{Re}(\lambda_{\max}(\tilde{A}_{\mathrm{transient}})) < \mathrm{Re}(\lambda_{\min}(\tilde{A}_{\mathrm{ref}}))$*, and* $u(t) = \phi_{\mathrm{tracking}}(\pi_{\mathrm{tracking}}(t,x(t)), e(t), \tilde{K}(t))$*, then* $\tilde{e}(\cdot)$ *and* $\tilde{K}(\cdot)$ *are uniformly bounded. Moreover,* $\tilde{e}(t) \in \mathring{\tilde{\mathcal{E}}}$*,* $t \geq t_0$*,* $\|y(t) - C_{\mathrm{p}}x_{\mathrm{p}}(t)\| \to 0$ *and* $\|y(t) - \tilde{C}\tilde{x}_{\mathrm{ref}}(t)\| \to 0$ *as* $t \to \infty$ *uniformly in* $t_0 \in [0,\infty)$*, and* $\alpha_{\max}(\tilde{e}(\cdot)) \geq \alpha$ *with* $\alpha > -\mathrm{Re}(\lambda_{\min}(\tilde{A}_{\mathrm{ref}})) \geq -\mathrm{Re}(\lambda_{\max}(\tilde{A}_{\mathrm{ref}}))$*. Lastly,* $\|y(t) - y_{\mathrm{cmd}}(t)\|$*,* $t \geq t_0$*, is uniformly bounded.*

Proof: The result follows as in the proof of Theorem II.2 as is omitted for brevity. ∎

Similarly to Theorem II.2, the control law (38) reduces to an adaptive controller deduced by applying Theorem III.1. Furthermore, the control law (38) and the adaptive laws (39) and (40) guarantee that the plant measured output $y(\cdot)$ converges to $\tilde{C}\tilde{x}_{\mathrm{ref}}(\cdot)$ before the transient dynamics of the reference model (13) has decayed; Figure 3 provides a schematic representation of the architecture provided by Theorem III.2. Lastly, if $y_{\mathrm{cmd}}(\cdot)$ varies sufficiently slowly, then the plant measured output $y(\cdot)$ converges to the reference signal $y_{\mathrm{cmd}}(\cdot)$.

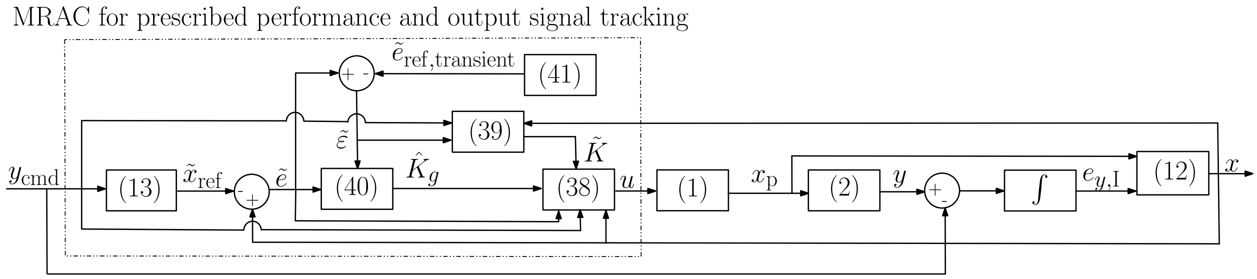

Fig. 3 Graphical representation of the MRAC for prescribed performance architecture presented in Theorem III.2. Applying the control law (38) **and the adaptive laws** (39) **and** (40)**, Theorem III.2 guarantees uniform boundedness of both the closed-loop system's trajectory error** $\tilde{e}(\cdot)$ **and the adaptive gain matrices** $\tilde{K}(\cdot)$ **and** $\hat{K}_g(\cdot)$**. Moreover, Theorem III.2 guarantees uniform asymptotic convergence of** $y(\cdot)$ **to** $\tilde{C}\tilde{x}_{\mathrm{ref}}(\cdot)$**. Lastly, Theorem III.2 guarantees that** $y(\cdot)$ **reaches** $y_{\mathrm{cmd}}(\cdot)$ **before the transient dynamics of the reference model** (13) **has decayed.**

IV. Modeling and Control of the Longitudinal Dynamics of a Quad-Biplane

A. Longitudinal dynamics of a quad-biplane

A quad-biplane is a biplane aircraft equipped with four propellers aligned with the vehicle's roll axis. This vehicle takes off and lands vertically like a conventional quadcopter and can fly horizontally like a conventional fixed-wing aircraft. To capture this tail-sitter's dynamics, we introduce an orthonormal *inertial reference frame* $\mathbb{I} \triangleq \{O; X, Y, Z\}$ such that the UAV's weight is captured by $F_g^{\mathbb{I}} = mgZ$, where $m > 0$ denotes the UAV's mass and $g > 0$ denotes the gravitational acceleration. For simplicity, we assume that the reference frame $\mathbb{I}$ is fixed with the Earth; this assumption is realistic since a tail-sitter UAV flies at a Mach number less than 3 and, for the applications considered in this paper, its maximum altitude is considerably lower than 10km [41, Ch. 2]. We also introduce an orthonormal *body reference frame* $\mathbb{J}(\cdot) \triangleq \{A(\cdot); x_{\mathrm{body}}(\cdot), y_{\mathrm{body}}(\cdot), z_{\mathrm{body}}(\cdot)\}$ fixed with the UAV, where $A(\cdot)$ denotes the UAV's center of mass, $x_{\mathrm{body}} : [t_0, \infty) \to \mathbb{R}^3$ denotes the UAV's *roll axis* and $z_{\mathrm{body}} : [t_0, \infty) \to \mathbb{R}^3$ denotes the UAV's *yaw axis*. Finally, we introduce an orthonormal *wind reference frame* $\mathbb{W}(\cdot) \triangleq \{A(\cdot); x_{\mathrm{wind}}(\cdot), y_{\mathrm{wind}}(\cdot), z_{\mathrm{wind}}(\cdot)\}$ such that $x_{\mathrm{wind}}(\cdot)$ is collinear with the UAV's velocity vector relative to the freestream wind and, in case of zero freestream wind velocity, $z_{\mathrm{wind}}(t) = z_{\mathrm{body}}(t)$, $t \geq t_0$. Figure 4 shows a schematic representation of the reference frames $\mathbb{I}$, $\mathbb{J}(\cdot)$, and $\mathbb{W}(\cdot)$ under longitudinal flight assumptions.

Assume that the UAV is symmetric, the UAV moves in the plane containing the inertial X and Z axes, that is, $y_{\mathrm{body}}(t) \equiv Y$, $t \geq t_0$, and the UAV's velocity vector relative to the freestream wind is contained in its vertical plane of symmetry, that is, $x_{\mathrm{wind}}^{\mathrm{T}}(t) y_{\mathrm{body}}(t) = 0$. In this case, the UAV's *translational dynamic equations* are captured by

$$\ddot{x}_A(t) = m^{-1}\left[F_X^{\mathbb{I}}(t) - L(t, v(t)) \sin\gamma(t) - D(t, v(t)) \cos\gamma(t)\right], \qquad x_A(t_0) = x_{A,0}, \qquad \dot{x}_A(t_0) = x_{A,0,\mathrm{d}}, \qquad t \geq t_0, \tag{42}$$

$$\ddot{z}_A(t) = m^{-1}\left[-F_Z^{\mathbb{I}}(t) + mg - L(t, v(t)) \cos\gamma(t) + D(t, v(t)) \sin\gamma(t)\right], \qquad z_A(t_0) = z_{A,0}, \qquad \dot{z}_A(t_0) = z_{A,0,\mathrm{d}}, \tag{43}$$

where $x_A : [t_0, \infty) \to \mathbb{R}$ and $z_A : [t_0, \infty) \to \mathbb{R}$ denote the UAV's position along the inertial X and Z axes, respectively,

$$F_X^{\mathbb{I}}(t) \triangleq (T_{\mathrm{upper}}(t) + T_{\mathrm{lower}}(t)) \cos\theta(t), \tag{44}$$

$$F_Z^{\mathbb{I}}(t) \triangleq (T_{\mathrm{upper}}(t) + T_{\mathrm{lower}}(t)) \sin\theta(t) \tag{45}$$

denote the components of the *thrust force* produced by the propellers along the X and Z axes, respectively, $T_{\mathrm{upper}} : [t_0, \infty) \to \mathbb{R}$ denotes the sum of the thrust forces produced by the two propellers placed at a distance $l > 0$ along the $-z_{\mathrm{body}}(\cdot)$ direction, $T_{\mathrm{lower}} : [t_0, \infty) \to \mathbb{R}$ denotes the sum of the thrust forces produced by the two propellers placed at a distance l along the $z_{\mathrm{body}}(\cdot)$ direction, $L(t, v) \triangleq \frac{1}{2}\rho\|v\|^2 S C_l(\alpha(t))$ denotes the *lift force* produced by the UAV, $\rho > 0$ denotes the *air density*, $S > 0$ denotes the *wing planform area*, $v(t) \triangleq [\dot{x}_A(t), 0, \dot{z}_A(t)]^{\mathrm{T}}$ denotes the *UAV velocity vector* relative to the freestream wind, $C_l : \mathbb{R} \to \mathbb{R}$ denotes the *aerodynamic lift coefficient*, $\alpha(t) \triangleq \mathrm{atan2}\,(\dot{z}_A(t), \dot{x}_A(t))$ denotes the UAV's *angle of attack*, $\mathrm{atan2}\,(\cdot, \cdot)$ denotes the *signed inverse tangent function*, $D(t, v) \triangleq \frac{1}{2}\rho\|v\|^2 S C_d(\alpha(t))$ denotes the *aerodynamic drag* produced by the UAV, $C_d : \mathbb{R} \to \mathbb{R}$ denotes the *aerodynamic drag coefficient*, $\gamma(t) \triangleq \theta(t) - \alpha(t)$

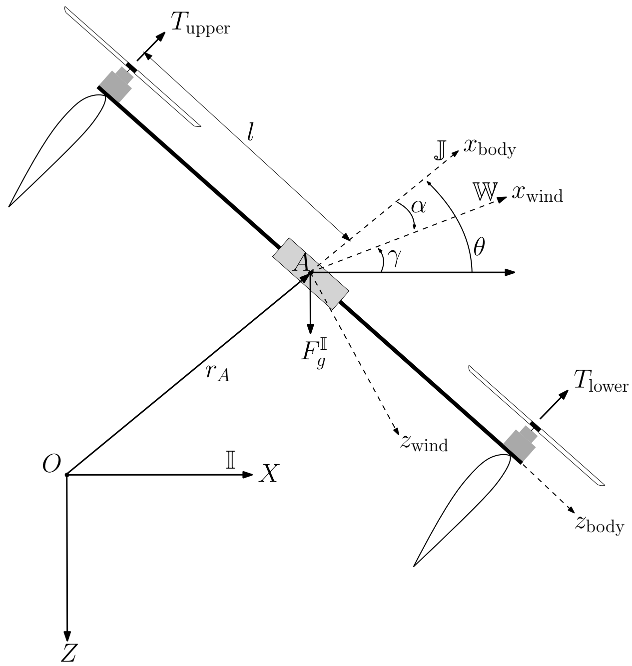

Fig. 4 Schematic, bi-dimensional representation of the quad-biplane UAV shown in Figure 1, and inertial, body, and wind reference frames.

denotes the UAV's *flight path angle*, and $\theta : [t_0, \infty) \to \mathbb{R}$ denotes the UAV's *pitch angle*. We remark that since the UAV's velocity with respect to the freestram wind is contained in the UAV's plane of symmetry, the UAV's pitch angle does not need to be constrained within the interval $\left(-\frac{\pi}{2}, \frac{\pi}{2}\right)$ [41, pp. 18-19], and the UAV's sideslip angle is identically equal to zero [41, p. 40].

Assuming that the UAV moves in the plane containing the inertial X and Z axes, that is, $x_{\text{body}}^{\mathrm{T}}(t)\omega(t) \equiv 0$, $t \geq t_0$, and $z_{\text{body}}^{\mathrm{T}}(t)\omega(t) \equiv 0$, where $\omega : [t_0, \infty) \to \mathbb{R}^3$ denotes the *angular velocity* of the body reference frame $\mathbb{J}(\cdot)$ with respect to the inertial reference frame $\mathbb{I}$ [41, Def. 1.9], the *rotational dynamic equation* is given by

$$\ddot{\theta}(t) = I_y^{-1}\left[M_y(t) - M_a(t, v(t))\right], \qquad \theta(t_0) = \theta_0, \qquad \dot{\theta}(t_0) = \theta_{0,\mathrm{d}}, \qquad t \geq t_0, \tag{46}$$

where $I_y > 0$ denotes the *principal moment of inertia* of the UAV about the $y_{\text{body}}(\cdot)$ axis,

$$M_y(t) \triangleq l\left[T_{\text{lower}}(t) - T_{\text{upper}}(t)\right] \tag{47}$$

denotes the *moment of the thrust force* exerted by the UAV propellers, $M_a(t, v) \triangleq \frac{1}{2}\rho\|v\|^2 SlC_m(\alpha(t))$ denotes the denotes the *aerodynamic moment* produced by the UAV, and $C_m : \mathbb{R} \to \mathbb{R}$ denotes the *aerodynamic moment coefficient*. In this paper, we assume that the quad-biplane is not equipped with mobile surfaces such as ailerons or flaps to generate a pitching moment, but only relies on the propellers' differential thrust to generate the required control moment. It is worthwhile to remark that (46) also approximates the quad-biplane's rotational dynamics in the longitudinal plane whenever the components of the UAV's angular velocity vector along the $x_{\text{body}}(\cdot)$ and $z_{\text{body}}(\cdot)$ axes are arbitrarily small, that is, $x_{\text{body}}^{\mathrm{T}}(t)\omega(t) \approx 0$, $t \geq t_0$, and $z_{\text{body}}^{\mathrm{T}}(t)\omega(t) \approx 0$ [41, p. 44].

B. Control strategy for the longitudinal dynamics of a quad-biplane

The longitudinal dynamics of a quad-biplane, whose control input is exclusively provided by the propellers' thrust force, that is, $T_{\text{upper}}(\cdot)$ and $T_{\text{lower}}(\cdot)$, is underactuated. To verify this fact, we recall the definition of actuation and underactuation of the nonlinear dynamical system

$$\ddot{q}(t) = f(t, q(t), \dot{q}(t)) + G(q(t))u(t), \qquad q(t_0) = q_0, \qquad \dot{q}(t_0) = q_{0,\mathrm{d}}, \qquad t \geq t_0, \tag{48}$$

where $q : [t_0, \infty) \to \mathbb{R}^n$, $u : [t_0, \infty) \to \mathbb{R}^m$, $f : [t_0, \infty) \times \mathbb{R}^n \times \mathbb{R}^n \to \mathbb{R}^n$ is continuous in $t \in [t_0, \infty)$ and Lipschitz continuous in $(q, \dot{q}) \in \mathbb{R}^n \times \mathbb{R}^n$, and $G : \mathbb{R}^n \to \mathbb{R}^{n \times m}$ is Lipschitz continuous in $q \in \mathbb{R}^n$.

Definition IV.1 *[42, Def. 2.9] Consider the dynamical system given by* (48). *If* $\operatorname{rank} G(q) = n$ *for all* $q \in \mathcal{D} \subseteq \mathbb{R}^n$*, then* (48) *is actuated on* $\mathcal{D}$. *Alternatively, if* $\operatorname{rank} G(q) < n$ *for all* $q \in \mathcal{D}$*, then* (48) *is underactuated on* $\mathcal{D}$.

The second-order nonlinear dynamical system given by (42), (43), and (46) is in the same form as (48) with $n = 3$, $m = 2$, $q = [x_A, z_A, \theta]^{\mathrm{T}}$, $u = \left[T_{\mathrm{upper}}, T_{\mathrm{lower}}\right]^{\mathrm{T}}$,

$$f(t, q, \dot{q}) = \begin{bmatrix} -m^{-1}\left(L(t,v)\sin\gamma(t) + D(t,v)\cos\gamma(t)\right) \\ g + m^{-1}\left(D(t,v)\sin\gamma(t) - L(t,v)\cos\gamma(t)\right) \\ -I_y^{-1} M_a(t,v) \end{bmatrix}, \qquad (t, q, \dot{q}) \in [t_0, \infty) \times \mathbb{R}^3 \times \mathbb{R}^3, \tag{49}$$

$$G(q) = \begin{bmatrix} m^{-1}\cos\theta & m^{-1}\cos\theta \\ -m^{-1}\sin\theta & -m^{-1}\sin\theta \\ -l I_y^{-1} & l I_y^{-1} \end{bmatrix}. \tag{50}$$

Thus, it follows from Definition IV.1 and (50) that the longitudinal dynamics of quad-biplanes is underactuated for all $q \in \mathbb{R}^3$. In light of this consideration, we propose the following control strategy based on an outer loop and an inner loop. The user defines a continuously differentiable and bounded reference trajectory along both the inertial X axis and the inertial Z axis, that is, $x_{A,\mathrm{user}} : [t_0, \infty) \to \mathbb{R}$ and $z_{A,\mathrm{user}} : [t_0, \infty) \to (-\infty, 0]$, respectively. Thus, the outer loop is designed to compute the components of the thrust force such that $x_A(t)$, $t \geq t_0$, and $z_A(t)$ track $x_{A,\mathrm{user}}(t)$ and $z_{A,\mathrm{user}}(t)$, respectively. Thus, the components of the thrust force needed to follow $x_{A,\mathrm{user}}(t)$ and $z_{A,\mathrm{user}}(t)$ determines the command pitch angle $\theta_{\mathrm{cmd}}(t)$, $t \geq t_0$, that is, the desired direction of the thrust force. Finally, the inner loop computes the moment of the thrust force $M_y(t)$, $t \geq t_0$, such that $\theta(t)$ tracks $\theta_{\mathrm{cmd}}(t)$.

C. Outer loop design

In this paper, we assume that the aerodynamic lift, drag, and moment coefficients are modeled as

$$C_d(\alpha) = C_{d,0} + C_{d,\alpha}\alpha, \qquad \alpha \in \mathbb{R}, \tag{51}$$

$$C_l(\alpha) = C_{l,0} + C_{l,\alpha}\alpha, \tag{52}$$

$$C_m(\alpha) = C_{m,0} + C_{m,\alpha}\alpha, \tag{53}$$

where $C_{d,0} > 0$, $C_{l,0} \geq 0$, $C_{m,0} \geq 0$, $C_{d,\alpha} > 0$, $C_{l,\alpha} \in \mathbb{R}$, and $C_{m,\alpha} \in \mathbb{R}$. This model is usually valid only for small angles of attack, and the user-defined reference trajectories is not necessarily designed to verify these assumptions. However, we rely on the ability of the MRAC law for prescribed performance to meet the user-defined constraints on the trajectory tracking error despite parametric uncertainties. Furthermore, any alternative model, whereby the aerodynamic forces and moments can be expressed as linear combinations of known functions of the state vector by means of unknown constant coefficients, can be applied to the proposed framework; examples of such models may be deduced from piecewise polynomial interpolation of experimental data as done, for instance, in [7]. In this paper, we also assume that the wing planform area S, the air density ρ, and the aerodynamic coefficients $C_{d,0}$, $C_{l,0}$, $C_{m,0}$, $C_{d,\alpha}$, $C_{l,\alpha}$, and $C_{m,\alpha}$ are unknown and estimated by $\hat{S} > 0$, $\hat{\rho} > 0$, $\hat{C}_{d,0} > 0$, $\hat{C}_{l,0} \in \mathbb{R}$, $\hat{C}_{m,0} \in \mathbb{R}$, $\hat{C}_{d,\alpha} > 0$, $\hat{C}_{l,\alpha} \in \mathbb{R}$, and $\hat{C}_{m,\alpha} \in \mathbb{R}$, respectively.

Under these modeling assumptions, (42) and (43) are equivalent to

$$\begin{aligned} \dot{x}_{\mathrm{outer}}(t) = A_{\mathrm{outer}} x_{\mathrm{outer}}(t) + B_{\mathrm{outer}} \begin{bmatrix} F_X^{\mathbb{I}}(t) \\ -F_Z^{\mathbb{I}}(t) \end{bmatrix} \\ + B_{\mathrm{outer}} \begin{bmatrix} -\frac{1}{2}\rho\|v(t)\|^2 S\left[(C_{l,0} + C_{l,\alpha}\alpha(t))\sin\gamma(t) + (C_{d,0} + C_{d,\alpha}\alpha(t))\cos\gamma(t)\right] \\ mg + \frac{1}{2}\rho\|v(t)\|^2 S\left[(C_{d,0} + C_{d,\alpha}\alpha(t))\sin\gamma(t) - (C_{l,0} + C_{l,\alpha}\alpha(t))\cos\gamma(t)\right] \end{bmatrix}, \\ x_{\mathrm{outer}}(t_0) = \left[x_{A,0}, \theta_0, x_{A,0,\mathrm{d}}, \theta_{0,\mathrm{d}}\right]^{\mathrm{T}}, \qquad t \geq t_0, \end{aligned} \tag{54}$$

where $x_{\mathrm{outer}}(t) \triangleq [x_A(t), z_A(t), \dot{x}_A, \dot{z}_A(t)]^{\mathrm{T}}$, $A_{\mathrm{outer}} = \begin{bmatrix} 0_{2\times 2} & I_2 \\ 0_{2\times 2} & 0_{2\times 2} \end{bmatrix}$, and $B_{\mathrm{outer}} = m^{-1}\begin{bmatrix} 0_{2\times 2} \\ I_2 \end{bmatrix}$. Therefore, if

$$F_X^{\mathbb{I}}(t) = u_{\mathrm{outer},1}(t) + \frac{1}{2}\hat{\rho}\|v(t)\|^2 \hat{S}\left[(\hat{C}_{l,0} + \hat{C}_{l,\alpha}\alpha(t))\sin\gamma(t) + (\hat{C}_{d,0} + \hat{C}_{d,\alpha}\alpha(t))\cos\gamma(t)\right], \qquad t \geq t_0 \tag{55}$$

$$-F_Z^{\mathbb{I}}(t) = u_{\text{outer},2}(t) - \frac{1}{2}\hat{\rho}\|v(t)\|^2\hat{S}(\hat{C}_{d,0} + \hat{C}_{d,\alpha}\alpha(t))\sin\gamma(t), \tag{56}$$

then (54) reduces to

$$\dot{x}_{\text{outer}}(t) = A_{\text{outer}}x_{\text{outer}}(t) + B_{\text{outer}}\left[u_{\text{outer}}(t) + \Theta_{\text{outer}}^{\mathrm{T}}\Phi_{\text{outer}}(t)\right],$$
$$x_{\text{outer}}(t_0) = \left[x_{A,0}, z_{A,0}, x_{A,0,\text{d}}, z_{A,0,\text{d}}\right]^{\mathrm{T}}, \qquad t \geq t_0, \tag{57}$$

where $u_{\text{outer}}(t) \triangleq \left[u_{\text{outer},1}(t), u_{\text{outer},2}(t)\right]^{\mathrm{T}} \in \mathbb{R}^2$ denotes the *virtual control input*, and expressions for $\Theta_{\text{outer}} \in \mathbb{R}^{5\times 2}$ and $\Phi_{\text{outer}}(t) \in \mathbb{R}^5$ are provided in the Appendix.

After having computed $u_{\text{outer}}(\cdot)$ according to the procedure discussed in Section IV.E below so that $x_A(t)$, $t \geq t_0$, and $z_A(t)$ track $x_{A,\text{user}}(t)$ and $z_{A,\text{user}}(t)$, respectively, and $F_X^{\mathbb{I}}(\cdot)$ and $F_Z^{\mathbb{I}}(\cdot)$ are deduced from (55) and (56), respectively. Furthermore, the *command pitch angle*, that is, the pitch angle the aircraft should track, is defined as

$$\theta_{\text{cmd}}(t) \triangleq \begin{cases} \operatorname{atan2}\left(F_Z^{\mathbb{I}}(t), F_X^{\mathbb{I}}(t)\right), & \text{if } \left|F_X^{\mathbb{I}}(t)\right| > \varepsilon_X \text{ and } F_Z^{\mathbb{I}}(t) - mg > \varepsilon_Z, \\ \operatorname{atan2}\left(\left|F_Z^{\mathbb{I}}(t)\right|, F_X^{\mathbb{I}}(t)\right), & \text{if } \left|F_X^{\mathbb{I}}(t)\right| > \varepsilon_X \text{ and } F_Z^{\mathbb{I}}(t) - mg \leq -\varepsilon_Z, \\ \operatorname{atan2}\left(|F_Z^{\mathbb{I}}(t)|, F_X^{\mathbb{I}}(t)\right), & \text{if } F_X^{\mathbb{I}}(t) \leq -\varepsilon_X \text{ and } |F_Z^{\mathbb{I}}(t) - mg| \leq \varepsilon_Z, \\ \operatorname{atan2}\left(\left|F_Z^{\mathbb{I}}(t)\right|, F_X^{\mathbb{I}}(t)\right), & \text{if } \left|F_X^{\mathbb{I}}(t)\right| \leq \varepsilon_X \text{ and } |F_Z^{\mathbb{I}}(t) - mg| > \varepsilon_Z, \\ \frac{\pi}{2}, & \text{if } |F_X^{\mathbb{I}}(t)| \leq \varepsilon_X \text{ and } \left|F_Z^{\mathbb{I}}(t) - mg\right| \leq \varepsilon_Z, \end{cases} \qquad t \geq t_0, \tag{58}$$

where $\varepsilon_X > 0$, $\varepsilon_Z > 0$, and $\operatorname{atan2}(\cdot,\cdot)$ denotes the signed inverse tangent function. The command pitch angle $\theta_{\text{cmd}}(t)$, $t \geq t_0$, captures the direction of the thrust force so that the UAV follows the user-defined trajectory and the propellers never point downwards; this is a safety precaution so that if the UAV must gain altitude rapidly, then the propellers are already pointed in the desired direction for a prompt response. The user-defined constants ε_X and ε_Z capture the fact that commercial-off-the-shelf motors for small UAVs do not allow to produce arbitrarily small thrust forces. Furthermore, ε_X and ε_Z serve as safety margins. Indeed, if the horizontal component of the thrust force is small, that is $\left|F_X^{\mathbb{I}}(t)\right| \leq \varepsilon_X$, $t \geq t_0$, and $\left|F_Z^{\mathbb{I}}(t)\right| > \varepsilon_Z$, then the command pitch angle may rapidly switch between values in some neighborhood of 0 and values in some neighborhood of π, and the inner loop's controller would be overly stressed. Equation (58) is designed to prevent this rapid switching from occurring. Similarly, if $\left|F_X^{\mathbb{I}}(t)\right| \leq \varepsilon_X$, $t \geq t_0$, and $\left|F_Z^{\mathbb{I}}(t)\right| \leq \varepsilon_Z$, then the command pitch angle may rapidly switch between values in neighborhoods of 0 and π and between values in neighborhoods of $\pi/2$ and $-\pi/2$. Equation (58) is designed to prevent this rapid switching from occurring. Lastly, if $F_X^{\mathbb{I}}(t) = F_Z^{\mathbb{I}}(t) = 0$, $t \geq t_0$, then $\operatorname{atan2}(F_Z^{\mathbb{I}}(t), F_X^{\mathbb{I}}(t))$ is unspecified. Consequently, the quad-biplane may be pointed downward whenever the propellers are turned on again, which may cause a sudden and undesired loss of altitude.

D. Inner loop design

The UAV's pitch dynamics (46) is equivalent to

$$\dot{x}_{\text{inner}}(t) = A_{\text{inner}}x_{\text{inner}}(t) + B_{\text{inner}}\left[M_y(t) - \frac{1}{2}\rho\|v(t)\|^2 Sl\left(C_{m,0} + C_{m,\alpha}\alpha(t)\right)\right],$$
$$x_{\text{inner}}(t_0) = \left[\theta_0, \theta_{0,\text{d}}\right]^{\mathrm{T}}, \qquad t \geq t_0, \tag{59}$$

where $x_{\text{inner}}(t) \triangleq \left[\theta(t), \dot{\theta}(t)\right]^{\mathrm{T}}$, $A_{\text{inner}} \triangleq \begin{bmatrix} 0 & 1 \\ 0 & 0 \end{bmatrix}$, and $B_{\text{inner}} \triangleq \begin{bmatrix} 0 \\ I_y^{-1} \end{bmatrix}$. Therefore, if

$$M_y(t) = u_{\text{inner}}(t) + \frac{1}{2}\hat{\rho}\|v(t)\|^2\hat{S}l\left(\hat{C}_{m,0} + \hat{C}_{m,\alpha}\alpha(t)\right), \qquad t \geq t_0, \tag{60}$$

then (59) reduces to

$$\dot{x}_{\text{inner}}(t) = A_{\text{inner}}x_{\text{inner}}(t) + B_{\text{inner}}\left[u_{\text{inner}}(t) + \Theta_{\text{inner}}^{\mathrm{T}}\Phi_{\text{inner}}(t)\right], \qquad x_{\text{inner}}(t_0) = \left[\theta_0, \theta_{0,\text{d}}\right]^{\mathrm{T}}, \qquad t \geq t_0, \tag{61}$$

where expressions for $\Theta_{\text{inner}} \in \mathbb{R}^2$ and $\Phi_{\text{inner}}(t) \in \mathbb{R}^2$ are provided in the Appendix. The virtual control input $u_{\text{inner}}(t)$, $t \geq t_0$, is computed according to the procedure discussed in Section IV.E below so that $\theta(t)$ tracks $\theta_{\text{cmd}}(t)$ given by (58). Thus, $M_y(t)$, $t \geq t_0$, is deduced from (60).

E. Inner and outer loops integration

The dynamical models that capture inner and outer loops, that is, (61) and (57), respectively, can be integrated and reduced to the same form as (1) and (2) with $n = 6$, $m = 3$, $N = 7$, $x_{\rm p}(t) = \left[x_{\rm inner}^{\rm T}(t), x_{\rm outer}^{\rm T}(t)\right]^{\rm T}$, $t \geq t_0$, $u(t) = \left[u_{\rm inner}^{\rm T}(t), u_{\rm outer}^{\rm T}(t)\right]^{\rm T}$, $A_{\rm p} = \text{blockdiag}\left(A_{\rm inner}, A_{\rm outer}\right)$, $B_{\rm p} = \begin{bmatrix} B_{\rm inner} & 0_4 \\ 0_{2\times 2} & B_{\rm outer}\end{bmatrix}$, $C_{\rm p} = \begin{bmatrix} [1,0] & 0_{1\times 2} & 0_{1\times 2} \\ 0_{2\times 2} & I_2 & 0_{2\times 2}\end{bmatrix}$, $D_{\rm p} \in \mathbb{R}^{3\times 3}\backslash\{0_{3\times 3}\}$ arbitrary, $\Theta = \begin{bmatrix} \Theta_{\rm inner}^{\rm T} & 0_2 \\ 0_6^{\rm T} & \Theta_{\rm outer}^{\rm T}\end{bmatrix}^{\rm T}$, and $\Phi(t, x_p) = \left[\Phi_{\rm inner}^{\rm T}(t), \Phi_{\rm outer}^{\rm T}(t)\right]^{\rm T}$. Thus, Theorems II.1 and III.1 can be applied to find feedback control laws for $u(\cdot)$ such that $[\theta(t), x_A(t), z_A(t)]^{\rm T}$, $t \geq t_0$, tracks the trajectory of the reference model (3) with $A_{\rm ref} = \text{blockdiag}\left(A_{\rm ref,inner}, A_{\rm ref,outer}\right)$, $A_{\rm ref,inner} \triangleq \begin{bmatrix} 0 & 1 \\ -K_{P,\rm inner} & -K_{D,\rm inner}\end{bmatrix}$, $A_{\rm ref,outer} \triangleq \begin{bmatrix} 0_{2\times 2} & I_2 \\ -K_{P,\rm outer} & -K_{D,\rm outer}\end{bmatrix}$, $K_{P,\rm inner}$ and $K_{D,\rm inner} > 0$ user-defined, $K_{P,\rm outer}$ and $K_{D,\rm outer} \in \mathbb{R}^{2\times 2}$ symmetric, positive-definite, and user-defined, $B_{\rm ref} = \begin{bmatrix} \begin{bmatrix} 0 \\ 1 \end{bmatrix} & 0_{2\times 2} \\ 0_2 & 0_{2\times 2} \\ 0_2 & I_2 \end{bmatrix}$, and

$$r(t) = \begin{bmatrix} K_{P,\rm inner}\theta_{\rm cmd}(t) + K_{D,\rm inner}\dot{\theta}_{\rm cmd}(t) + \ddot{\theta}_{\rm cmd}(t) \\ K_{P,\rm outer}\begin{bmatrix} x_{A,\rm user}(t) \\ z_{A,\rm user}(t)\end{bmatrix} + K_{D,\rm outer}\begin{bmatrix} \dot{x}_{A,\rm user}(t) \\ \dot{z}_{A,\rm user}(t)\end{bmatrix} + \begin{bmatrix} \ddot{x}_{A,\rm user}(t) \\ \ddot{z}_{A,\rm user}(t)\end{bmatrix}\end{bmatrix}, \qquad t \geq t_0.$$

The complexity of this approach, however, lays in employing differentiators to estimate both $\dot{\theta}_{\rm cmd}(t)$, $t \geq t_0$, and $\ddot{\theta}_{\rm cmd}(t)$, since the first and second time derivatives of $\theta_{\rm cmd}(t)$ can not be computed analytically from (58). Alternatively, Theorems II.2 and III.2 can be applied to find feedback control laws for $u(\cdot)$ such that $y_1(t) = \theta(t)$, $t \geq t_0$, tracks $\theta_{\rm cmd}(t)$ given by (58), $y_2(t) = x_A(t)$ tracks $x_{A,\rm user}(t)$, and $y_3(t) = z_A(t)$ tracks $z_{A,\rm user}(t)$. Remarkably, this approach based on output signal tracking does not require computing the derivatives of $x_{A,\rm user}(t)$, $z_{A,\rm user}(t)$, and $\theta_{\rm cmd}(t)$.

F. Thrust force realization

The total thrust force needed to realize $F_X^{\mathbb{I}}(t)$, $t \geq t_0$, $F_Z^{\mathbb{I}}(t)$, and $M_y(t)$ given by (55), (56), and (60), respectively, can be determined at each time instant as a solution of the optimization problem

$$\begin{aligned} \min \quad & T(t), \\ \text{s.t.} \quad & T(t)\cos\theta(t) = F_X^{\mathbb{I}}(t), \\ & T(t)\sin\theta(t) = F_Z^{\mathbb{I}}(t), \\ & T(t) = T_{\rm upper}(t) + T_{\rm lower}(t), \\ & [T_{\rm lower}(t) - T_{\rm upper}(t)]l = M_y(t), \\ & T_{\rm upper}(t) \geq 0, \\ & T_{\rm lower}(t) \geq 0. \end{aligned}$$

However, this linear program may not have a solution since the UAV may be oriented in the wrong direction. Moreover, the resulting control policy may be overly aggressive and produce large oscillations in the transient phase and in the absence of a framework able to impose *a priori* user-defined bounds on the tracking error.

In this paper, the thrust force is computed as

$$\hat{T}(t) \triangleq \begin{cases} \dfrac{\sqrt{\left(F_X^{\mathbb{I}}(t)\right)^2 + \left(F_Z^{\mathbb{I}}(t)\right)^2}}{\cos\left(\theta_{\rm cmd}(t) - \theta(t)\right)}, & \text{if } |\theta_{\rm cmd}(t) - \theta(t)| < \theta_{\max} \quad \text{and} \quad F_Z^{\mathbb{I}}(t) \geq 0, \qquad t \geq t_0, \\ \dfrac{\left|F_X^{\mathbb{I}}(t)\right|}{\cos\left(\theta_{\rm cmd}(t) - \theta(t)\right)}, & \text{if } |\theta_{\rm cmd}(t) - \theta(t)| < \theta_{\max} \quad \text{and} \quad F_Z^{\mathbb{I}}(t) < 0, \\ \sqrt{\left(F_X^{\mathbb{I}}(t)\right)^2 + \left(F_Z^{\mathbb{I}}(t)\right)^2}, & \text{otherwise,} \end{cases} \tag{62}$$

where $\theta_{\max} \in \left[0, \frac{\pi}{2}\right)$ is a user-defined tolerance on the maximum attitude error. The thrust force $\hat{T}(t)$, $t \geq t_0$, and the moment of the thrust force $M_y(t)$ are realized by the UAV's propellers by setting

$$T_{\rm upper}(t) = \begin{cases} 0, & \text{if } \hat{T}(t) < \dfrac{M_y(t)}{l} \text{ and } M_y(t) > 0, \qquad t \geq t_0, \\ -\dfrac{M_y(t)}{l} & \text{if } \hat{T}(t) < -\dfrac{M_y(t)}{l} \text{ and } M_y(t) < 0, \\ \dfrac{\hat{T}(t)}{2} - \dfrac{M_y(t)}{2l}, & \text{if } \hat{T}(t) \geq \dfrac{|M_y(t)|}{l} \text{ and } |\theta_{\rm cmd}(t) - \theta(t)| \leq \theta_{\max}, \\ 0, & \text{if } \hat{T}(t) \geq \dfrac{|M_y(t)|}{l} \text{ and } \theta_{\rm cmd}(t) - \theta(t) > \theta_{\max}, \\ \dfrac{|M_y(t)|}{l}, & \text{if } \hat{T}(t) \geq \dfrac{|M_y(t)|}{l} \text{ and } \theta_{\rm cmd}(t) - \theta(t) < -\theta_{\max}, \end{cases} \tag{63}$$

and

$$T_{\rm lower}(t) = \begin{cases} \dfrac{M_y(t)}{l}, & \text{if } \hat{T}(t) < \dfrac{M_y(t)}{l} \text{ and } M_y(t) > 0, \\ 0 & \text{if } \hat{T}(t) < -\dfrac{M_y(t)}{l}, \text{ and } M_y(t) < 0, \\ \dfrac{\hat{T}(t)}{2} + \dfrac{M_y(t)}{2l}, & \text{if } \hat{T}(t) \geq \dfrac{|M_y(t)|}{l} \text{ and } |\theta_{\rm cmd}(t) - \theta(t)| \leq \theta_{\max}, \\ \dfrac{|M_y(t)|}{l}, & \text{if } \hat{T}(t) \geq \dfrac{|M_y(t)|}{l} \text{ and } \theta_{\rm cmd}(t) - \theta(t) > \theta_{\max}, \\ 0, & \text{if } \hat{T}(t) \geq \dfrac{|M_y(t)|}{l} \text{ and } \theta_{\rm cmd}(t) - \theta(t) < -\theta_{\max}. \end{cases} \tag{64}$$

Equations (62) and (58) can be interpreted as follows. If the UAV must produce some thrust force upward, that is, in the $-Z$ direction, and $\theta(t)$, $t \geq t_0$, is sufficiently close to $\theta_{\rm cmd}(t)$, that is, if $|\theta_{\rm cmd}(t) - \theta(t)| < \theta_{\max}$, then $\hat{T}(t)$ guarantees that the projection of the thrust force along the direction captured by $\theta_{\rm cmd}(t)$ equals the required thrust force, that is, $\sqrt{\left(F_X^{\mathbb{I}}(t)\right)^2 + \left(F_Z^{\mathbb{I}}(t)\right)^2}$. Alternatively, if the UAV must produce some thrust in the Z direction, and $|\theta_{\rm cmd}(t) - \theta(t)| < \theta_{\max}$, $t \geq t_0$, then $\hat{T}(t)$ is designed to realize the projection of $F_X^{\mathbb{I}}(t)$ along the direction captured by $\theta_{\rm cmd}(t)$, and gravity is exploited to let the quad-biplane descend; this approach prevents the propellers from pointing downward. Finally, if the difference between $\theta(t)$, $t \geq t_0$, and $\theta_{\rm cmd}(t)$ is sufficiently large, that is, if $|\theta_{\rm cmd}(t) - \theta(t)| \geq \theta_{\max}$, then $\hat{T}(t)$ is set to realize the desired moment of the thrust force $M_y(t)$ given by (60) so that $\theta(t)$ tracks $\theta_{\rm cmd}(t)$, while the required thrust force $\sqrt{\left(F_X^{\mathbb{I}}(t)\right)^2 + \left(F_Z^{\mathbb{I}}(t)\right)^2}$ is realized. Equations (63) and (64) guarantee that the thrust force produced by the propellers is always non-negative. Furthermore, (63) and (64) guarantee that the required moment of the thrust force $M_y(\cdot)$ is always realized. Figure 5 provides a schematic representation of the architecture to control the longitudinal dynamics of quad-biplanes proposed in this paper.

V. Numerical Simulations

In this section, we present the results of two sets of numerical simulations using the control laws presented in Sections II and III, and the control architecture presented in Section IV. These results highlight the efficacy of the proposed MRAC laws for prescribed performance over classical MRAC laws for both state and output signal tracking. Furthermore, these results verify the applicability of the control architecture for quad-biplanes. These simulations are performed considering the custom-designed quad-biplane shown in Figure 1.

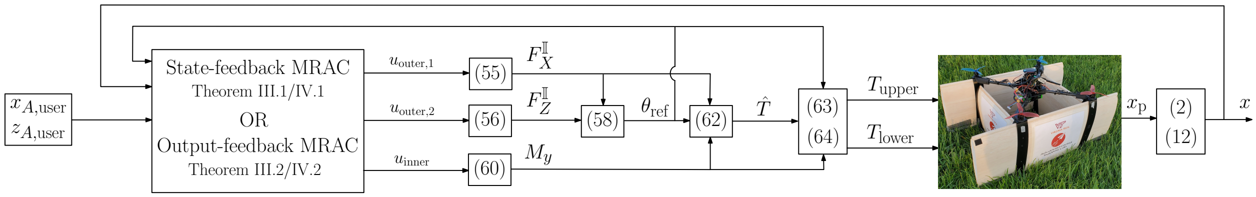

Fig. 5 Schematic representation of the architecture to control the longitudinal dynamics of quad-biplanes by means of MRAC laws for state tracking and output signal tracking. The control laws and the adaptive laws proposed by Theorem II.1 or Theorem III.1 can be applied to compute control inputs for the state tracking architecture, and Theorem II.2 or Theorem III.2 can be applied to compute control inputs for the output signal tracking architecture.

Table 1 Dynamic properties, aerodynamic coefficients, and estimated aerodynamic coefficients of the quad-biplane shown in Figure 1.

Parameter	Value	Units	Parameter	Value	Units	Parameter	Value	Units	Parameter	Value	Units
m	2.000	kg	$\theta_{\max}$	35.00	deg	$C_{l,0}$	0.000	-	$\hat{C}_{l,0}$	0.010	-
I_y	0.080	kg·m^2	ε_X	1.962	N	$C_{d,0}$	0.100	-	$\hat{C}_{d,0}$	0.080	-
l	0.500	m	ε_Z	1.962	N	$C_{m,0}$	0.000	-	$\hat{C}_{m,0}$	0.020	-
ρ	1.225	kg/m^3	$\hat{\rho}$	1	kg/m^3	$C_{l,\alpha}$	0.070	-	$\hat{C}_{l,\alpha}$	0.037	-
S	0.500	m^2	$\hat{S}$	0.500	m^2	$C_{d,\alpha}$	0.170	-	$\hat{C}_{d,\alpha}$	0.106	-
κ_{inner}	0.017	-	κ_{outer}	10	-	$C_{m,\alpha}$	0.010	-	$\hat{C}_{m,\alpha}$	0.000	-

A. State Tracking

In this section, we present the results of numerical simulations that demonstrate the efficacy of the control law presented in Theorem III.1 and the architecture outlined in Section IV. These results are compared with simulation results obtained by applying the classical MRAC control law for state tracking given by Theorem II.1. These results show how user-defined levels of performance can be imposed *a priori* on the longitudinal dynamics of a quad-biplane despite uncertainties in aerodynamic coefficients and despite the complexity of realizing the desired thrust force and moment of the thrust force, while always pointing the propellers either horizontally or upward. To further challenge the ability of these MRAC laws to produce satisfactory results, in this section we assume that $\dot{\theta}_{\mathrm{cmd}}(t) = \ddot{\theta}_{\mathrm{cmd}}(t) \equiv 0$, $t \geq t_0$, while $\theta_{\mathrm{cmd}}(t)$ is given by (58) and hence, is not necessarily constant. Both sets of simulations are performed by employing the modeling parameters shown in Table 1.

For the results presented in this section, the user-defined reference trajectory is given by

$$x_{A,\mathrm{user}}(t) = \begin{cases} 0, & \text{if } 0 \leq t < 2.5, \\ 4.9t, & \text{if } 2.5 \leq t < 5, \\ 4.9t, & \text{if } 5 \leq t < 25, \\ 110, & \text{if } 25 \leq t < 42, \\ 110, & \text{if } 42 \leq t < 45, \\ 110, & \text{otherwise,} \end{cases} \qquad z_{A,\mathrm{user}}(t) = \begin{cases} -0.4t, & \text{if } 0 \leq t < 2.5, \\ -0.4t, & \text{if } 2.5 \leq t < 5, \\ -2, & \text{if } 5 \leq t < 25, \\ -2, & \text{if } 25 \leq t < 42, \\ -2 + \dfrac{2(t-42)}{3}, & \text{if } 42 \leq t < 45, \\ 0, & \text{otherwise,} \end{cases} \qquad t \geq t_0. \tag{65}$$

This user-defined reference trajectory was chosen to demonstrate the efficacy of the proposed control architecture in VTOL, traditional, and transition flight regimes. The speed of the user-defined trajectory in the forward flight phase was chosen so that the weight of the quad-biplane was not necessarily compensated using the lift generated by its wings. In both sets of simulations, the initial conditions are given by $\left[\theta_0, \theta_{0,\mathrm{d}}\right]^{\mathrm{T}} = [\frac{\pi}{2}, 0]^{\mathrm{T}}$ and $\left[x_{A,0}, z_{A,0}, x_{A,0,\mathrm{d}}, z_{A,0,\mathrm{d}}\right]^{\mathrm{T}} = 0_4$. The user-defined constraints on the trajectory tracking error are captured by

$$h_e(e^{\mathrm{T}} M e) = \kappa_{\mathrm{outer}}^2 + \kappa_{\mathrm{inner}}^2 - e^{\mathrm{T}} M e, \qquad e \in \mathbb{R}^6, \tag{66}$$

where κ_{inner} and κ_{outer} are given in Table 1. The parameters underlying the classical MRAC law for state tracking and the MRAC law for prescribed performance and state tracking are given in the Appendix.

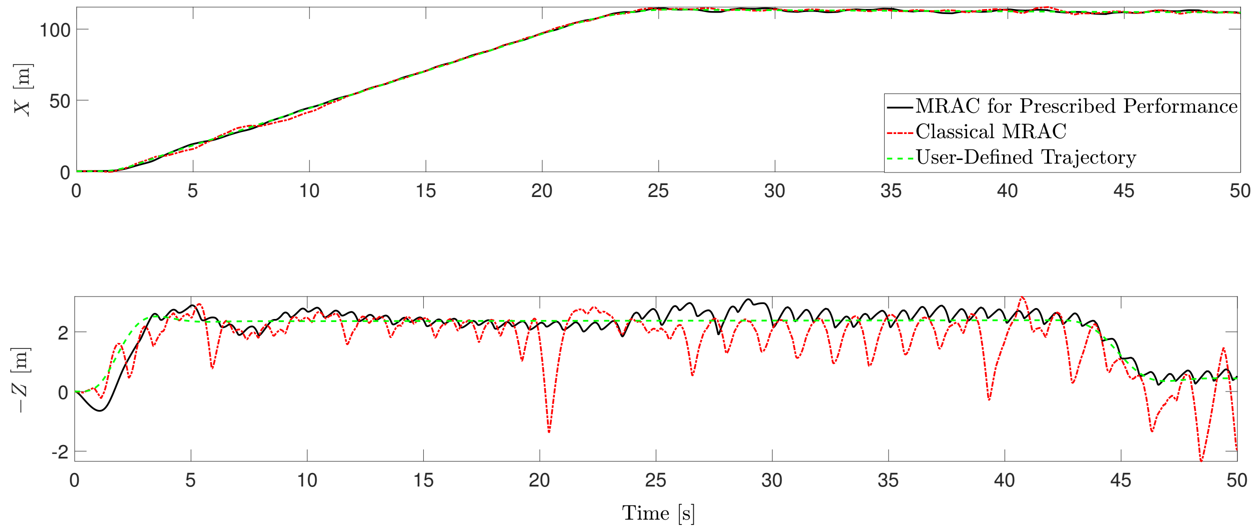

Fig. 6 Trajectory of a quad-biplane applying the MRAC law for prescribed performance and state tracking presented in Theorem III.1 and the classical MRAC law presented in Theorem II.1. Although both control laws guarantee satisfactory trajectory tracking performance along the horizontal direction, the MRAC law for prescribed performance outperforms the classical MRAC law while tracking the user-defined trajectory in the vertical direction.

Figure 6 shows UAV's trajectory as a functions of time obtained by applying the control laws outlined by Theorems II.1 and III.1 and the proposed control architecture. Although both classical MRAC and MRAC for prescribed performance produce good trajectory tracking along the horizontal direction, the MRAC law for prescribed performance guarantees a smaller trajectory tracking error than the classical MRAC law along the vertical direction. Figure 7 shows the resulting path; a zoomed-in portion of this figure shows the UAV's path at the end of the forward flight stage and upon landing. It is apparent that, by applying the MRAC law for prescribed performance, the UAV's path oscillates considerably less than by applying a classical MRAC law. Furthermore, the tight margins on the tracking error imposed by the MRAC law for prescribed performance guarantee that the UAV's altitude is never negative. While applying the classical MRAC law, the UAV's altitude descends below $Z = 0$. Figure 8 shows the pitch angle and the command pitch angle obtained by applying Theorem III.1 and Theorem II.1. By applying the MRAC law for prescribed performance, the UAV's pitch angle follows the command pitch angle very closely, whereas by applying the classical MRAC law, the UAV's pitch angle angle follows the command pitch angle less accurately. Figure 9 shows the weighted norm on the trajectory tracking error for the outer and inner loops, that is, $e^{\mathrm{T}}_{\mathrm{outer}}(t)M_{\mathrm{outer}}e_{\mathrm{outer}}(t)$, $t \geq t_0$, and $e^{\mathrm{T}}_{\mathrm{inner}}(t)M_{\mathrm{inner}}e_{\mathrm{inner}}(t)$, where $e(t) = \left[e^{\mathrm{T}}_{\mathrm{inner}}(t), e^{\mathrm{T}}_{\mathrm{outer}}(t)\right]^{\mathrm{T}}$ and $M = \mathrm{blockdiag}\left(M_{\mathrm{inner}}, M_{\mathrm{outer}}\right)$. Despite the classical MRAC law, the MRAC law for prescribed performance does not violate these user-defined constraints. By applying the control law outlined in Theorem II.1, the $\mathcal{L}_2$-norm of the trajectory tracking error is 2.15 and $\mathcal{L}_\infty$-norm of the trajectory tracking error is 9.92. Applying the control law outlined in Theorem III.1, the $\mathcal{L}_2$-norm of the trajectory tracking error is 1.87 and the $\mathcal{L}_\infty$-norm of the trajectory tracking error is 5.11. Thus, as anticipated by the analysis of Figures 6–9, applying the MRAC law for prescribed performance, both the average and the maximum trajectory tracking errors are smaller than the average and the maximum trajectory tracking errors obtained by applying the classical MRAC law.

Figure 10 shows the control input computed by the MRAC law for prescribed performance and state tracking and that of the classical MRAC law. For being able to follow the reference trajectory more closely, the MRAC law for prescribed performance requires a considerably smaller control effort.

B. Output Tracking

In this section, we present the results of numerical simulations that demonstrate the efficacy of the control law presented in Theorem III.2 and the architecture outlined in Section IV despite uncertainties on aerodynamic coefficients and despite the complexity of realizing the desired thrust force and moment of the thrust force, while always pointing the propellers either horizontally or upward. The modeling parameters employed in these simulations are listed in Table

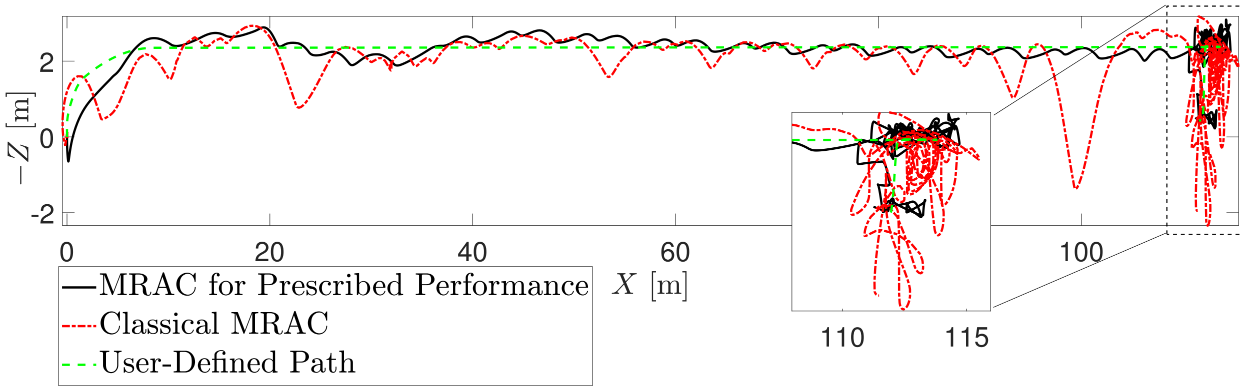

Fig. 7 User-defined reference path and path of a quad-biplane controlled by employing the MRAC law for prescribed performance and state tracking presented in Theorem III.1 and the classical MRAC law presented in Theorem II.1. The MRAC law for prescribed performance follows the reference trajectory more closely and clearly outperforms the classical MRAC law. As shown by the subfigure, during the landing stage, The MRAC law for prescribed performance guarantees considerably smaller oscillations in the UAV's position than the classical MRAC law. Furthermore, the quad-biplane's is always above ground.

Table 2 Parameters characterizing the quad-biplane in the output tracking simulations. The first and fourth columns list the parameters; the second and fifth columns list the value of each parameter; lastly, the third and sixth column lists the parameter's unit of measurement, if any.

Parameter	Value	Units	Parameter	Value	Units	Parameter	Value	Units	Parameter	Value	Units
m	2.000	kg	$\theta_{\max}$	35.00	deg	$C_{l,0}$	0.005	-	$\hat{C}_{l,0}$	0.010	-
I_y	0.080	kg·m^2	ε_X	1.962	N	$C_{d,0}$	0.100	-	$\hat{C}_{d,0}$	0.080	-
l	0.500	m	ε_Z	1.962	N	$C_{m,0}$	0.001	-	$\hat{C}_{m,0}$	0.020	-
ρ	1.225	kg/m^3	$\hat{\rho}$	1	kg/m^3	$C_{l,\alpha}$	0.100	-	$\hat{C}_{l,\alpha}$	0.037	-
S	0.500	m^2	$\hat{S}$	0.500	m^2	$C_{d,\alpha}$	0.150	-	$\hat{C}_{d,\alpha}$	0.106	-
D_p	I_3	-	κ	$\sqrt{35}$	-	$C_{m,\alpha}$	0.010	-	$\hat{C}_{m,\alpha}$	0.000	-

2, the control parameters are given in the Appendix, and the user-defined reference trajectory is given by

$$x_{A,\text{user}}(t) = \begin{cases} 0, & \text{if } 0 \leq t < 10, \\ 0, & \text{if } 10 \leq t < 30, \\ 13, & \text{if } 30 \leq t < 32, \\ 13 + 10(t-32), & \text{if } 32 \leq t < 52, \\ 213, & \text{if } 52 \leq t < 72, \\ 213, & \text{if } 72 \leq t < 82, \\ 213, & \text{otherwise,} \end{cases} \quad z_{A,\text{user}}(t) = \begin{cases} 0, & \text{if } 0 \leq t < 10, \\ -4, & \text{if } 10 \leq t < 30, \\ -4 & \text{if } 30 \leq t < 32, \\ -4 & \text{if } 32 \leq t < 52, \\ -4, & \text{if } 52 \leq t < 72, \\ -4 + 0.4(t-72), & \text{if } 72 \leq t < 82, \\ 0, & \text{otherwise,} \end{cases} \quad t \geq t_0. \tag{67}$$

The initial conditions are given by $[\theta_0, \theta_{0,\mathrm{d}}]^\mathrm{T} = [\pi/2, 0]^\mathrm{T}$, $[x_{A,0}, z_{A,0}, x_{A,0,\mathrm{d}}, z_{A,0,\mathrm{d}}]^\mathrm{T} = 0_4$. The user-defined constraints on the tracking error are captured by

$$h_e(\tilde{e}^\mathrm{T}\tilde{M}\tilde{e}) = \kappa^2 - \tilde{e}^\mathrm{T}\tilde{M}\tilde{e}, \qquad \tilde{e} \in \mathbb{R}^9, \tag{68}$$

where κ is given in Table 2. Remarkably, despite best effort, it was not possible to complete any numerical simulation that allowed to follow the reference trajectory given by (67), while applying the classical control law outlined by Theorem II.2 and employing the same modeling parameters.

Figure 11 shows UAV's trajectory as a function of time, and Figure 12 shows the corresponding path. From these figures, it is apparent how the UAV rapidly converges to its reference trajectory and closely follows it until landing.

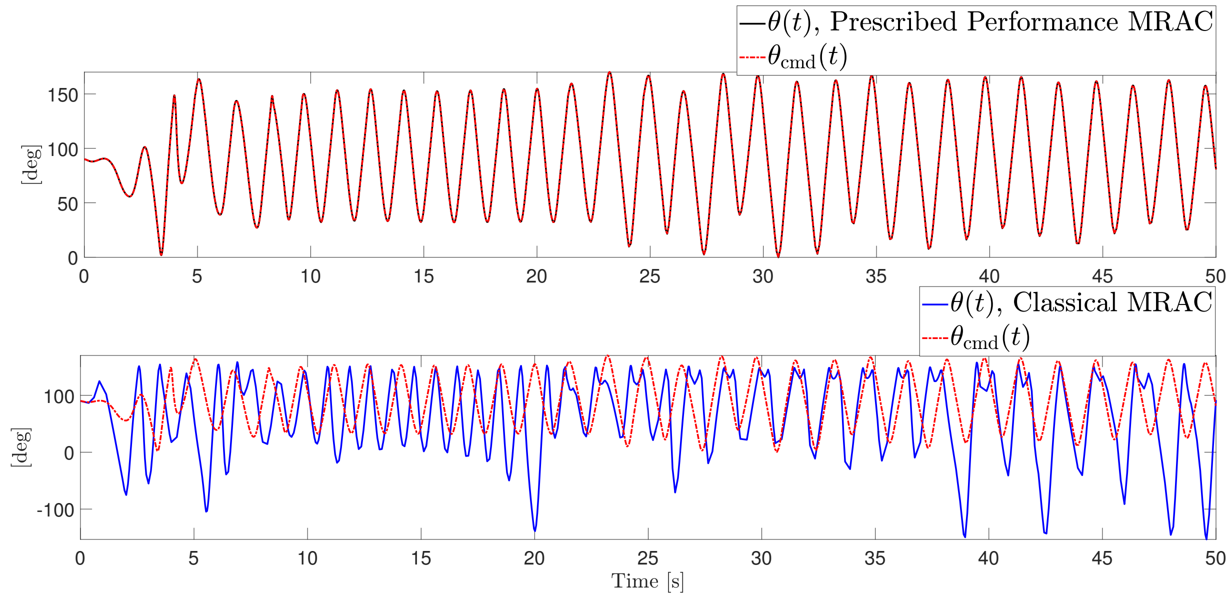

Fig. 8 Pitch angle of a quad-biplane applying the MRAC law for prescribed performance and state tracking presented in Theorem III.1 and the classical MRAC law presented in Theorem II.1. The MRAC law for prescribed performance clearly outperforms the classical MRAC law. In both cases, the pitch angle varies considerably. These oscillations are due to the fact that the UAV's reference trajectory is not designed to generate sufficient lift and maintain a constant altitude.

Figure 13 shows both the UAV's pitch angle and commanded pitch angle. Figure 14 shows the weighted norm on the tracking error, that is, $\tilde{e}^{\mathrm{T}}(t)\tilde{M}\tilde{e}(t)$, $t \geq t_0$. It is apparent how the user-defined constraints on the trajectory tracking error are always verified. The $\mathcal{L}_2$-norm of the augmented trajectory tracking error $\tilde{e}(\cdot)$ is 2.15. The $\mathcal{L}_\infty$-norm of the augmented trajectory tracking error is 4.50.

Figure 15 shows the control inputs, the thrust force $\hat{T}(\cdot)$ computed by applying (58), and the moment of the thrust force $M_y(\cdot)$ computed by applying (62). The forces and moments are compatible with the forces and moments that can be exerted by a UAV produced by commercial-off-the-shelf parts and whose relevant paramaters are listed in Table 2.

Lastly, Figure 16 shows the lift force $L(\cdot)$, the estimated lift force $\hat{L}(\cdot)$, the drag force $D(\cdot)$, the estimated drag force $\hat{D}(\cdot)$, the aerodynamic moment $M(\cdot)$, and the estimated aerodynamic moment $\hat{M}(\cdot)$. It is apparent how during the horizontal flight stage, the proposed control architecture exploits the UAV's aerodynamic forces to follow the user-defined reference trajectory.

VI. Conclusion

This paper presented a control architecture to regulate the longitudinal dynamics of a quad-biplane, which is actuated exclusively by its propellers. By applying this control architecture, the performance of the classical MRAC laws for state tracking are compared by means of numerical simulations with the performance of the MRAC laws for prescribed performance and state tracking, which were first introduced in [13]. This paper also presented for the first time MRAC laws for prescribed performance and output signal tracking, and showcased the ability of these control laws and of the proposed control architecture for quad-biplanes to track a user-defined reference trajectory. As demonstrated by the proposed numerical simulations, both MRAC for prescribed performance for state tracking and MRAC for prescribed performance for output signal tracking allow users to impose *a priori* constraints on both the trajectory tracking error and the rate of convergence of the closed-loop plant, while setting the adaptive rates arbitrarily, without modifying the user-defined reference trajectory, and without introducing estimators or differentiators.

Future work directions involve extending the results presented in this paper to control a quad-biplane without assuming symmetric flight conditions. Furthermore, the proposed results will be validated by means of flight tests. Preliminary flight test results can be found at [43].

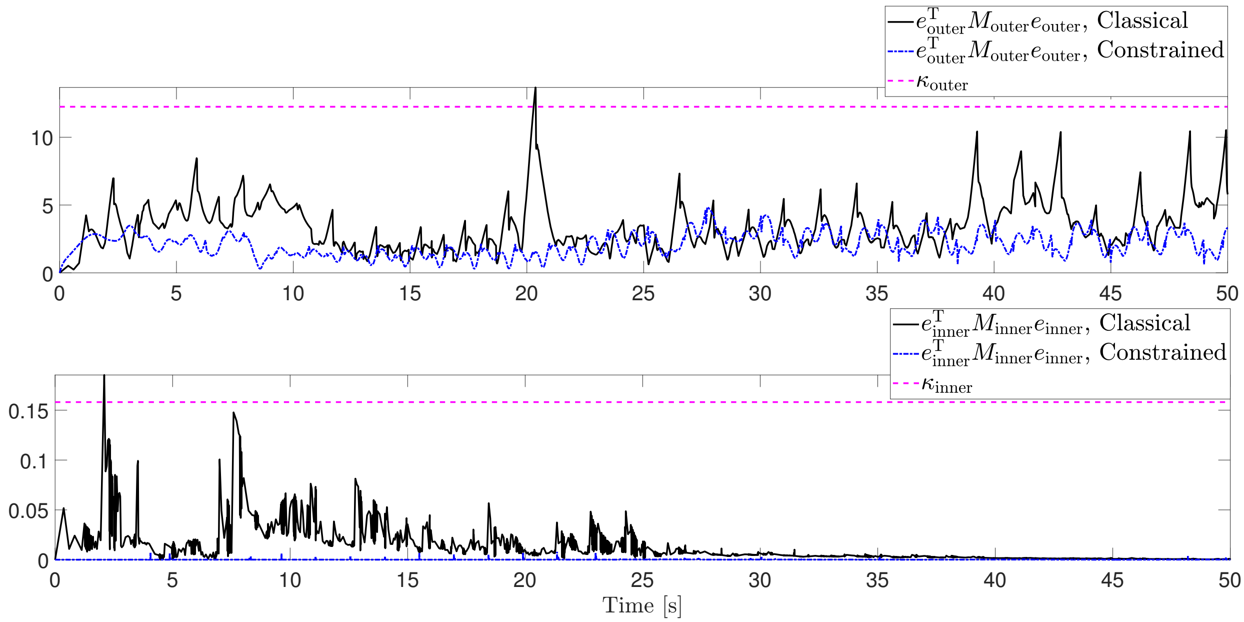

Fig. 9 Weighted norm of the trajectory tracking error obtained by applying Theorem II.1 and Theorem III.1. By applying the MRAC law for prescribed performance, the user-defined constraints on both the inner loop's and the outer loop's trajectory tracking error is never violated. By applying the classical MRAC law, these constraints are violated in multiple instances.

Acknowledgments

This work has been partly supported funded by the US Department of the Navy, Grant no. N004212110004, the Office of Naval Research, Grant no. N000141912422, and the Center for Unmanned Aircraft Systems (C-UAS), a National Science Foundation Industry/University Cooperative Research Center (I/UCRC) under NSF award No. CNS-1650465.

Appendix

Parameters of the matched uncertainties for the inner loop

Let $\Phi_{\mathrm{inner},i}(\cdot)$, $i = 1, 2$, denote the ith component of $\Phi_{\mathrm{inner}}(\cdot) \in \mathbb{R}^2$ in (61). Then,

$$\Phi_{\mathrm{inner},1}(t) \triangleq -\frac{l}{2}\|v(t)\|^2, \qquad t \geq t_0, \tag{69}$$

$$\Phi_{\mathrm{inner},2}(t) \triangleq -\frac{l}{2}\|v(t)\|^2\alpha(t), \tag{70}$$

Let $\Theta_{\mathrm{outer},(i)}(\cdot)$, $i = 1, 2$, denote the ith element of $\Theta_{\mathrm{outer}} \in \mathbb{R}^{5\times 2}$ in (61).

$$\Theta_{\mathrm{inner},1} \triangleq \rho S C_{m,0} - \hat{\rho}\hat{S}\hat{C}_{m,0}, \qquad t \geq t_0, \tag{71}$$

$$\Theta_{\mathrm{inner},2} \triangleq \rho S C_{m,\alpha} - \hat{\rho}\hat{S}\hat{C}_{m,\alpha}, \tag{72}$$

Parameters of the matched uncertainties for the outer loop

Let $\Phi_{\mathrm{outer},i}(\cdot)$, $i = 1, \ldots, 5$, denote the ith component of $\Phi_{\mathrm{outer}}(\cdot) \in \mathbb{R}^5$ in (57). Then,

$$\Phi_{\mathrm{outer},1}(t) \triangleq -\frac{1}{2}\|v(t)\|^2 \cos\gamma(t), \qquad t \geq t_0, \tag{73}$$

$$\Phi_{\mathrm{outer},2}(t) \triangleq -\frac{1}{2}\|v(t)\|^2 \cos\gamma(t)\alpha(t), \tag{74}$$

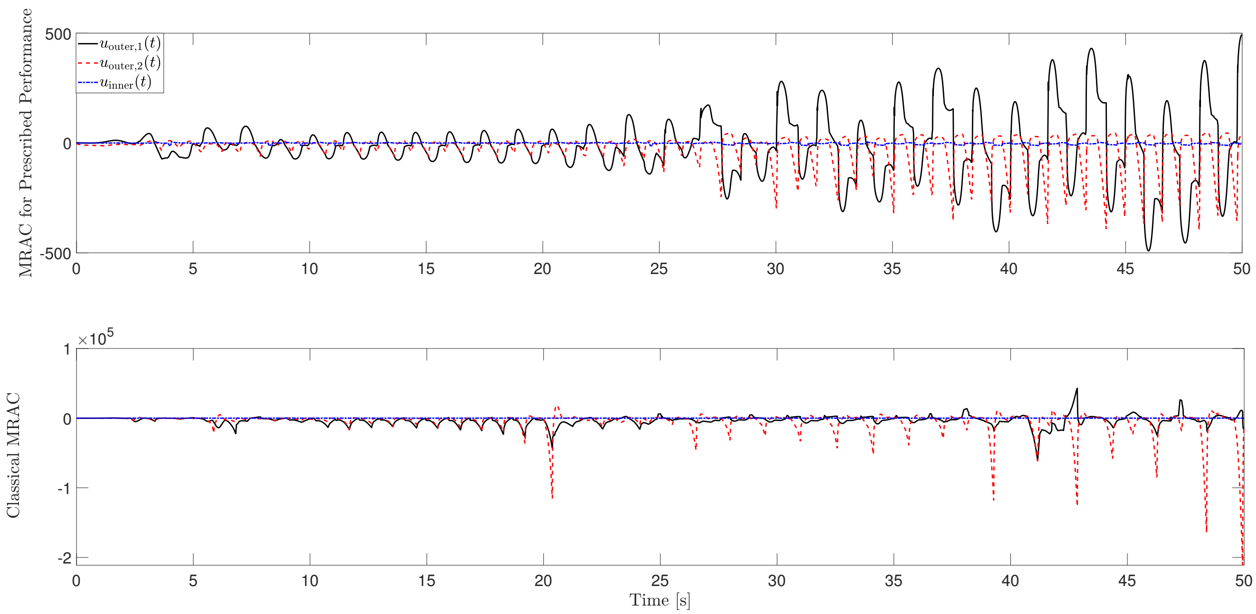

Fig. 10 Outer loop and inner loop control inputs computed by applying Theorems III.1 and II.1. The MRAC law for prescribed performance and state tracking requires less control effort than the classical MRAC law. The control input for the inner loop, $u_{\text{inner}}(\cdot)$, is relatively small for both control laws, since the vehicle's moment of inertia is small, and the aerodynamic moments are small as well.

$$\Phi_{\text{outer},3}(t) \triangleq -\frac{1}{2}\|v(t)\|^2 \sin\gamma(t), \tag{75}$$

$$\Phi_{\text{outer},4}(t) \triangleq -\frac{1}{2}\|v(t)\|^2 \sin\gamma(t)\alpha(t), \tag{76}$$

$$\Phi_{\text{outer},5}(t) \triangleq g. \tag{77}$$

Let
Then,

$$\Theta_{\text{outer},(1,1)} \triangleq \rho S C_{d,0} - \hat{\rho}\hat{S}\hat{C}_{d,0}, \qquad t \geq t_0, \tag{78}$$

$$\Theta_{\text{outer},(2,1)} \triangleq \rho S C_{d,\alpha} - \hat{\rho}\hat{S}\hat{C}_{d,\alpha}, \tag{79}$$

$$\Theta_{\text{outer},(3,1)} \triangleq \rho S C_{l,0} - \hat{\rho}\hat{S}\hat{C}_{l,0}, \tag{80}$$

$$\Theta_{\text{outer},(4,1)} \triangleq \rho S C_{l,\alpha} - \hat{\rho}\hat{S}\hat{C}_{l,\alpha}, \tag{81}$$

$$\Theta_{\text{outer},(5,1)} \triangleq 0, \tag{82}$$

$$\Theta_{\text{outer},(1,2)} \triangleq \rho S C_{l,0}, \tag{83}$$

$$\Theta_{\text{outer},(2,2)} \triangleq \rho S C_{l,\alpha}, \tag{84}$$

$$\Theta_{\text{outer},(3,2)} \triangleq \rho S C_{d,0} - \hat{\rho}\hat{S}\hat{C}_{d,0}, \tag{85}$$

$$\Theta_{\text{outer},(4,2)} \triangleq \rho S C_{d,\alpha} - \hat{\rho}\hat{S}\hat{C}_{d,\alpha}. \tag{86}$$

$$\Theta_{\text{outer},(5,2)} \triangleq m. \tag{87}$$

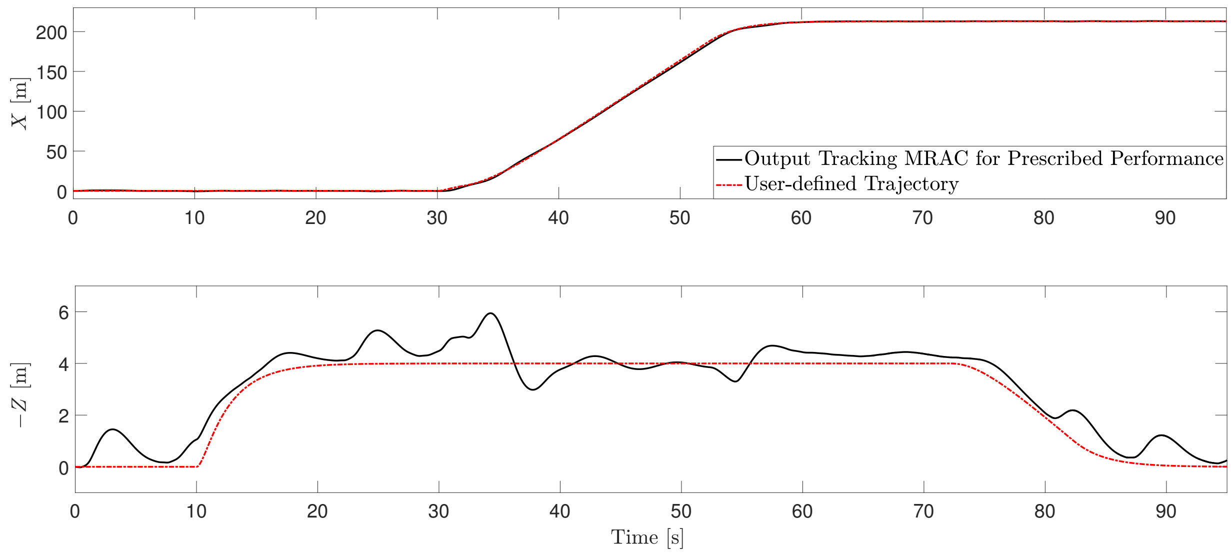

Fig. 11 Trajectory and reference trajectory of a quad-biplane applying the MRAC law for prescribed performance and output feedback tracking presented in Theorem III.2. The UAV follows the reference trajectory long the horizontal direction perfectly, whereas the trajectory tracking performance along the vertical direction suffers from some oscillations shortly after the transitions between horizontal and vertical flight modes. It was not possible to tune a control law based on Theorem II.2 and the proposed control architecture that allows the same quad-biplane to follow the same reference trajectory.

State Tracking Simulation Parameters

$$A_{\mathrm{ref,inner}} = \begin{bmatrix} 0 & 1 \\ -25 & -4 \end{bmatrix}, A_{\mathrm{ref,outer}} = \begin{bmatrix} 0 & 0 & 1 & 0 \\ 0 & 0 & 0 & 1 \\ -3 & 0 & -2 & 0 \\ 0 & -3 & 0 & -2 \end{bmatrix}, A_{\mathrm{ref}} = \mathrm{blockdiag}\left(A_{\mathrm{ref,inner}}, A_{\mathrm{ref,outer}}\right),$$

$$M = \begin{bmatrix} 70 & 1 & 0 & 0 & 0 & 0 \\ 1 & 3 & 0 & 0 & 0 & 0 \\ 0 & 0 & 3 & 0 & 1 & 0 \\ 0 & 0 & 0 & 6 & 0 & 1 \\ 0 & 0 & 1 & 0 & 1 & 0 \\ 0 & 0 & 0 & 1 & 0 & 1 \end{bmatrix}, A_{\mathrm{transient,inner}} = \begin{bmatrix} 0 & 1 \\ -4 \cdot 10^3 & -20 \end{bmatrix}, A_{\mathrm{transient,outer}} = \begin{bmatrix} 0 & 0 & 1 & 0 \\ 0 & 0 & 0 & 1 \\ -10^3 & 0 & -60 & 0 \\ 0 & -10^3 & 0 & -60 \end{bmatrix},$$

$$A_{\mathrm{transient}} = \mathrm{blockdiag}\left(A_{\mathrm{transient,inner}}, A_{\mathrm{transient,outer}}\right), \Gamma_{\mathrm{inner}} = 10^2 \cdot I_5, \Gamma_{\mathrm{outer}} = 50 \cdot I_{11}, \Gamma = \mathrm{blockdiag}\left(\Gamma_{\mathrm{inner}}, \Gamma_{\mathrm{outer}}\right),$$
$$\Gamma_g = \mathrm{diag}\left(150, 150, 10, 10, 10, 10\right).$$

Output Tracking Simulation Parameters

$$Q_{\mathrm{LQR}} = \mathrm{diag}(3 \cdot 10^3, 6 \cdot 10^3, 6 \cdot 10^3, 8, 1, 5 \cdot 10^4, 5 \cdot 10^4, 5, 5), R_{\mathrm{LQR}} = 0.5 \cdot I_3, Q_y = I_9,$$

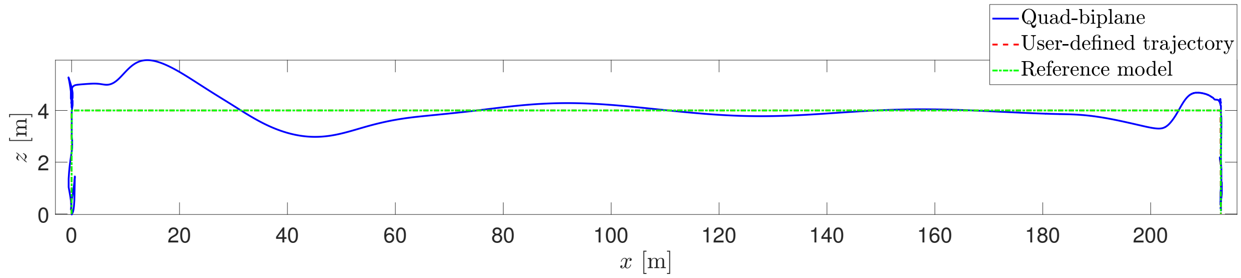

Fig. 12 User-defined reference path and path of a quad-biplane controlled by employing the MRAC law for prescribed performance and output signal tracking presented in Theorem III.2. Immediately after the initial ascent and transition to forward flight, the UAV follows its reference path with increasing precision.

$$\tilde{A}_{\text{transient}} = \begin{bmatrix} -10^4 \cdot I_3 & 0_{3\times1} & 0_3 & 0_3 & 0_3 & 0_3 & 0_3 \\ 0_{1\times3} & 0 & 1 & 0 & 0 & 0 & 0 \\ 0_{1\times3} & -5\cdot10^4 & -5\cdot10^2 & 0 & 0 & 0 & 0 \\ 0_{1\times3} & 0 & 0 & 0 & 0 & 1 & 0 \\ 0_{1\times3} & 0 & 0 & 0 & 0 & 0 & 1 \\ 0_{1\times3} & 0 & 0 & -5\cdot10^4 & 0 & -5\cdot10^2 & 0 \\ 0_{1\times3} & 0 & 0 & 0 & -5\cdot10^4 & 0 & -5\cdot10^2 \end{bmatrix},$$

$$\tilde{Q}_{\text{transient}} = I_9, \tilde{\Gamma} = \operatorname{diag}(10, 0.05, 0.05, 40, 40, 60, 60, 70, 70, 100)\cdot 10^3,$$

$$\tilde{\Gamma}_g = \operatorname{diag}\left(10^{-5}, 5^{-4}, 5^{-4}, 5, 0.5, 5, 8, 0.5, 0.5\right)\cdot 10^5,$$

$\tilde{M}$ is omitted for brevity and is computed by using an LMI solver.

References

[1] Tesla, N., "Method of aerial transportation," , September 1921. URL https://patents.google.com/patent/US1655113A/en, US Patent US1655113A.

[2] Garcia, O., Sanchez, A., Escareno, J., and Lozano, R., "Tail-sitter UAV having one tilting rotor: Modeling, Control and Real-Time Experiments," *IFAC Proceedings Volumes*, Vol. 41, No. 2, 2008, pp. 809–814.

[3] Knoebel, N. B., and McLain, T. W., "Adaptive quaternion control of a miniature tailsitter UAV," *American Control Conference*, 2008, pp. 2340–2345. https://doi.org/10.1109/ACC.2008.4586841.

[4] Argyle, M., Beard, R., and Morris, S., "The Vertical Bat tail-sitter: Dynamic model and control architecture," *American Control Conference*, 2013, pp. 806–811. https://doi.org/10.1109/ACC.2013.6579935.

[5] Oosedo, A., Abiko, S., Konno, A., and Uchiyama, M., "Optimal transition from hovering to level-flight of a quadrotor tail-sitter UAV," *Autonomous Robots*, Vol. 41, No. 5, 2017, pp. 1143–1159.

[6] Chiappinelli, R., and Nahon, M., "Modeling and Control of a Tailsitter UAV," *International Conference on Unmanned Aircraft Systems*, 2018, pp. 400–409. https://doi.org/10.1109/ICUAS.2018.8453301.

[7] Swarnkar, S., Parwana, H., Kothari, M., and Abhishek, A., "Biplane-quadrotor tail-sitter UAV: Flight dynamics and control," *Journal of Guidance, Control, and Dynamics*, Vol. 41, No. 5, 2018, pp. 1049–1067.

[8] Reddinger, J. P., McIntosh, K., Zhao, D., and Mishra, S., "Modeling and Trajectory Control of a Transitioning Quadrotor Biplane Tailsitter," *Vertical Flight Society Annual Forum*, 2019, pp. 1–11.

[9] McIntosh, K., Reddinger, J. P., Zhao, D., and Mishra, S., "Optimal Trajectory Generation for a Quadrotor Biplane Tailsitter," *Vertical Flight Society Annual Forum*, 2020, pp. 1–11.

[10] Swarnkar, S., Parwana, H., Kothari, M., and Abhishek, A., "Biplane-Quadrotor Tail-Sitter UAV: Flight Dynamics and Control," *Journal of Guidance, Control, and Dynamics*, Vol. 41, No. 5, 2018, pp. 1049–1067. https://doi.org/10.2514/1.G003201.

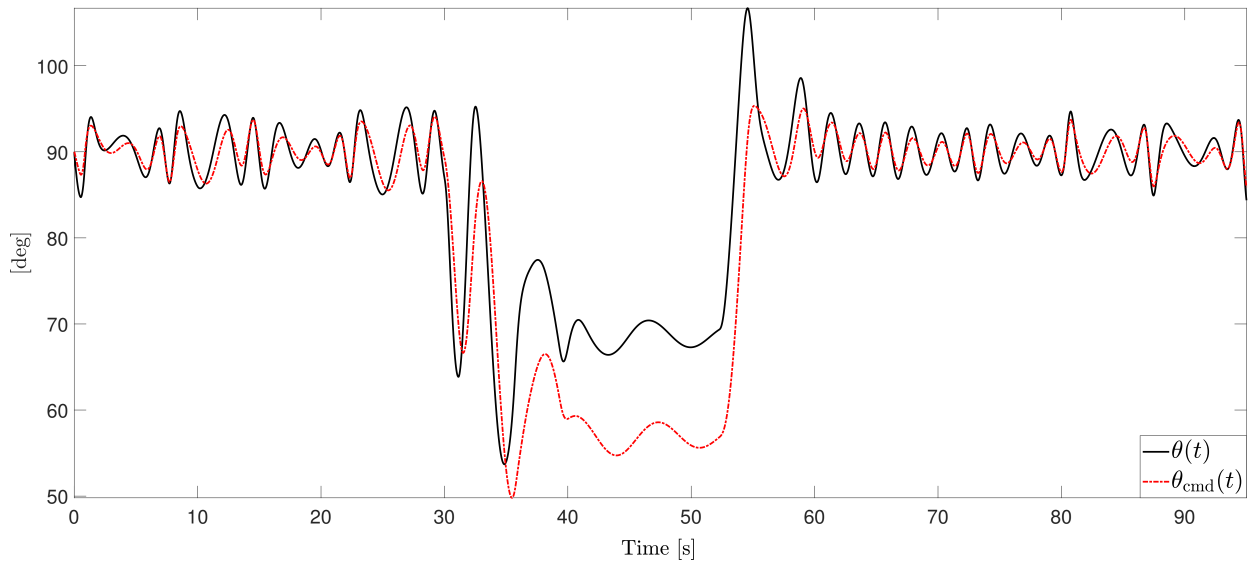

Fig. 13 Pitch angle and command pitch angle obtained by applying the MRAC law for prescribed performance and output signal tracking presented in Theorem III.2 and the proposed control architecture. Over the time intervals $[0, 30]$s and $[50, 95]$s, the quad-biplane is commanded to hover, and hence, the UAV's pitch angle is close to $\frac{\pi}{2}$. Over the time interval $(30, 50)$s, the quad-biplane is commanded to fly forward, and hence, the UAV's pitch angle approaches 50^{deg}.

[11] Raj, N., Simha, A., Kothari, M., Banavar, R. N., et al., "Iterative Learning based feedforward control for Transition of a Biplane-Quadrotor Tailsitter UAS," *2020 IEEE International Conference on Robotics and Automation (ICRA)*, IEEE, 2020, pp. 321–327.

[12] Lavretsky, E., and Wise, K., *Robust and Adaptive Control: With Aerospace Applications*, Springer, London, UK, 2012.

[13] Anderson, R. B., Marshall, J. A., and L'Afflitto, A., "Novel model reference adaptive control laws for improved transient dynamics and guaranteed saturation constraints," *Journal of the Franklin Institute*, Vol. 358, No. 12, 2021, pp. 6281–6308. https://doi.org/https://doi.org/10.1016/j.jfranklin.2021.06.020.

[14] Chowdhary, G., and Johnson, E. N., "Concurrent learning for convergence in adaptive control without persistency of excitation," *IEEE Conference on Decision and Control*, 2010, pp. 3674–3679. https://doi.org/10.1109/CDC.2010.5717148.

[15] Chowdhary, G., Yucelen, T., Mühlegg, M., and Johnson, E. N., "Concurrent learning adaptive control of linear systems with exponentially convergent bounds," *International Journal of Adaptive Control and Signal Processing*, Vol. 27, No. 4, 2013, pp. 280–301. https://doi.org/https://doi.org/10.1002/acs.2297.

[16] Chowdhary, G., Mühlegg, M., and Johnson, E. N., "Exponential parameter and tracking error convergence guarantees for adaptive controllers without persistency of excitation," *International Journal of Control*, Vol. 87, No. 8, 2014, pp. 1583–1603. https://doi.org/10.1080/00207179.2014.880128.

[17] Quindlen, J. F., Chowdhary, G., and How, J. P., "Hybrid model reference adaptive control for unmatched uncertainties," *American Control Conference*, 2015, pp. 1125–1130. https://doi.org/10.1109/ACC.2015.7170884.

[18] Pan, Y., Zhang, J., and Yu, H., "Model reference composite learning control without persistency of excitation," *IET Control Theory & Applications*, Vol. 10, No. 16, 2016, pp. 1963–1971.

[19] Datta, A., and Ioannou, P. A., "Performance analysis and improvement in model reference adaptive control," *IEEE Transactions on Automatic Control*, Vol. 39, No. 12, 1994, pp. 2370–2387. https://doi.org/10.1109/9.362856.

[20] Yang, J., Na, J., and Gao, G., "Robust adaptive control with a modified controller for transient response improvement," *International Conference on Modelling, Identification and Control*, 2017, pp. 929–934. https://doi.org/10.1109/ICMIC.2017.8321589.

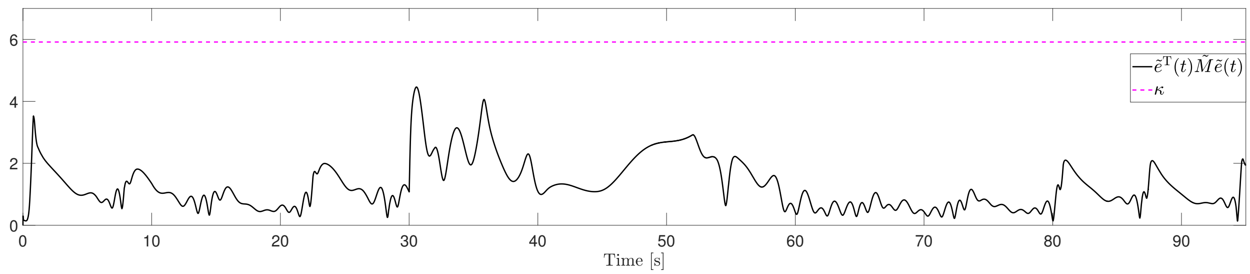

Fig. 14 Weighted norm of the trajectory tracking error obtained by applying Theorem III.2. For $t \in [0, 5)$s, $\tilde{e}^{\mathrm{T}}(t)\tilde{M}\tilde{e}(t)$ is large as the initial conditions for the adaptive gains are zero, and hence, the adaptive law must quickly adjust $\tilde{K}(t)$ and $\tilde{K}_g(t)$ to allow the quad-biplane to hover and follow the user-defined trajectory. For $t \in (30, 50)$s, $\tilde{e}^{\mathrm{T}}(t)\tilde{M}\tilde{e}(t)$ initially increases as the reference trajectory requires a sudden translation in the horizontal direction. Finally, for $t \in [50, 95]$s, that is, during the final hover and descent phase, $\tilde{e}^{\mathrm{T}}(t)\tilde{M}\tilde{e}(t)$ is small.

[21] Na, J., Herrmann, G., and Zhang, K., "Improving transient performance of adaptive control via a modified reference model and novel adaptation," *International Journal of Robust and Nonlinear Control*, Vol. 27, No. 8, 2017, pp. 1351–1372. https://doi.org/10.1002/rnc.3636.

[22] Yang, Y., Chen, X., and Li, C., "Transient performance improvement in model reference adaptive control using H_∞ optimal method," *Journal of the Franklin Institute*, Vol. 352, No. 1, 2015, pp. 16–32. https://doi.org/https://doi.org/10.1016/j.jfranklin.2014.09.014.

[23] Yucelen, T., De La Torre, G., and Johnson, E. N., "Improving transient performance of adaptive control architectures using frequency-limited system error dynamics," *International Journal of Control*, Vol. 87, No. 11, 2014, pp. 2383–2397. https://doi.org/10.1080/00207179.2014.922702.

[24] Gibson, T. E., Annaswamy, A. M., and Lavretsky, E., "On Adaptive Control With Closed-Loop Reference Models: Transients, Oscillations, and Peaking," *IEEE Access*, Vol. 1, 2013, pp. 703–717. https://doi.org/10.1109/ACCESS.2013.2284005.

[25] Yang, J., Liu, Y., Na, J., and Gao, G., *Improving Transient Performance of Modified Model Reference Adaptive Control*, Springer, Singapore, 2018, pp. 331–343. https://doi.org/10.1007/978-981-10-7212-3_21.

[26] Forshaw, J. L., Lappas, V. J., and Briggs, P., "Transitional Control Architecture and Methodology for a Twin Rotor Tailsitter," *Journal of Guidance, Control, and Dynamics*, Vol. 37, No. 4, 2014, pp. 1289–1298. https://doi.org/10.2514/1.G000314.

[27] Matsumoto, T., Kita, K., Suzuki, R., Oosedo, A., Go, K., Hoshino, Y., Konno, A., and Uchiyama, M., "A hovering control strategy for a tail-sitter VTOL UAV that increases stability against large disturbance," *IEEE International Conference on Robotics and Automation*, 2010, pp. 54–59. https://doi.org/10.1109/ROBOT.2010.5509183.

[28] Bilodeau, P.-R., and Wong, F., "Modeling and Control of a Hovering Mini Tail-Sitter," *International Journal of Micro Air Vehicles*, Vol. 2, No. 4, 2010, pp. 211–220. https://doi.org/10.1260/1756-8293.2.4.211.

[29] Hochstenbach, M., Notteboom, C., Theys, B., and Schutter, J. D., "Design and Control of an Unmanned Aerial Vehicle for Autonomous Parcel Delivery with Transition from Vertical Take-off to Forward Flight – VertiKUL, a Quadcopter Tailsitter," *International Journal of Micro Air Vehicles*, Vol. 7, No. 4, 2015, pp. 395–405. https://doi.org/10.1260/1756-8293.7.4.395.

[30] Lustosa, L. R., Defaÿ, F., and Moschetta, J.-M., "Longitudinal study of a tilt-body vehicle: Modeling, control and stability analysis," *International Conference on Unmanned Aircraft Systems*, 2015, pp. 816–824. https://doi.org/10.1109/ICUAS.2015.7152366.

[31] Ritz, R., and D'Andrea, R., "A global controller for flying wing tailsitter vehicles," *IEEE International Conference on Robotics and Automation*, 2017, pp. 2731–2738. https://doi.org/10.1109/ICRA.2017.7989318.

[32] Kita, K., Konno, A., and Uchiyama, M., "Transition between Level Flight and Hovering of a Tail-Sitter Vertical Takeoff and Landing Aerial Robot," *Advanced Robotics*, Vol. 24, No. 5-6, 2010, pp. 763–781. https://doi.org/10.1163/016918610X493570.

[33] Hajiloo, A., and Rodrigues, L., "Modeling and backstepping control of under-actuated spherical UAV," *IEEE Conference on Control Technology and Applications*, 2017, pp. 2069–2074. https://doi.org/10.1109/CCTA.2017.8062758.

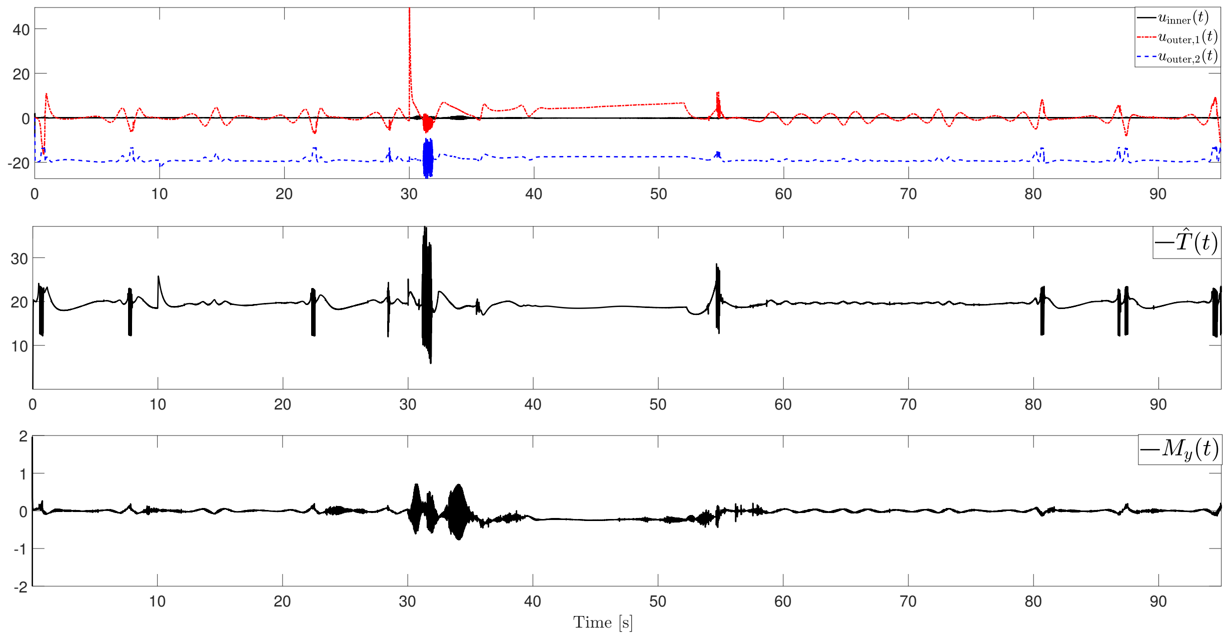

Fig. 15 Outer loop and inner loop control inputs computed by applying Theorem III.2. Over the time intervals $[0, 30]$s and $[50, 95]$s, the quad-biplane is commanded to hover, and hence, the control inputs, the thrust force, and the moment of the thrust force vary only by a small amount. Over these intervals, both the outer loop control input $u_{\text{outer},2}(\cdot)$ and the thrust force $\hat{T}(\cdot)$ are approximately equal to the weight of UAV in absolute value, and the inner loop control input $u_{\text{inner}}(\cdot)$ and moment of the thrust force $M_y(\cdot)$ are small. Over the time interval $(30, 50)$s, the quad-biplane is commanded to fly forward, and hence, the control inputs, the thrust force, and the moment of the thrust force vary considerably, The thrust force does not exceed 40N, which is feasible for most small quad-biplanes that have a thrust-to-weight ratio of two.

[34] Jung, Y., and Shim, D. H., "Development and Application of Controller for Transition Flight of Tail-Sitter UAV," *Journal of Intelligent & Robotic Systems*, Vol. 65, No. 1, 2012, pp. 137–152. https://doi.org/10.1007/s10846-011-9585-1.

[35] Zhang, S., Fei, Q., Liang, J., and Geng, Q., "Modeling and control for longitudinal attitude of a twin-rotor tail-sitter unmanned aerial vehicle," *IEEE International Conference on Control Automation*, 2017, pp. 816–821. https://doi.org/10.1109/ICCA.2017.8003165.

[36] Hrishikeshavan, V., Bawek, D., Rand, O., and Chopra, I., "Control of a quad rotor biplane micro air vehicle in transition from hover to forward flight," *American Helicopter Society Specialists Meeting on Unmanned Rotorcraft and Network Centric Operations*, AHS International Alexandria, VA, 2013.

[37] Theys, B., Notteboom, C., Hochstenbach, M., and De Schutter, J., "Design and control of an unmanned aerial vehicle for autonomous parcel delivery with transition from vertical take-off to forward flight," *International Journal of Micro Air Vehicles*, Vol. 7, No. 4, 2015, pp. 395–405.

[38] Wang, H., Zhao, X., Bai, H., Lu, C., Zhang, B., and Li, C., "Design of a Symmetrical Quad-rotor Biplane Tail-Sitter Aircraft without Control Surfaces and Experimental Verification," *MATEC Web of Conferences*, Vol. 151, EDP Sciences, 2018, p. 04009.

[39] Bechlioulis, C. P., and Rovithakis, G. A., "Robust Adaptive Control of Feedback Linearizable MIMO Nonlinear Systems With Prescribed Performance," *IEEE Transactions on Automatic Control*, Vol. 53, No. 9, 2008, pp. 2090–2099. https://doi.org/10.1109/TAC.2008.929402.

[40] Bechlioulis, C. P., and Rovithakis, G. A., "Adaptive control with guaranteed transient and steady state tracking error bounds for strict feedback systems," *Automatica*, Vol. 45, No. 2, 2009, pp. 532–538. https://doi.org/https://doi.org/10.1016/j.automatica.2008.08.012.

[41] L'Afflitto, A., *A Mathematical Perspective on Flight Dynamics and Control*, Springer, London, UK, 2017.

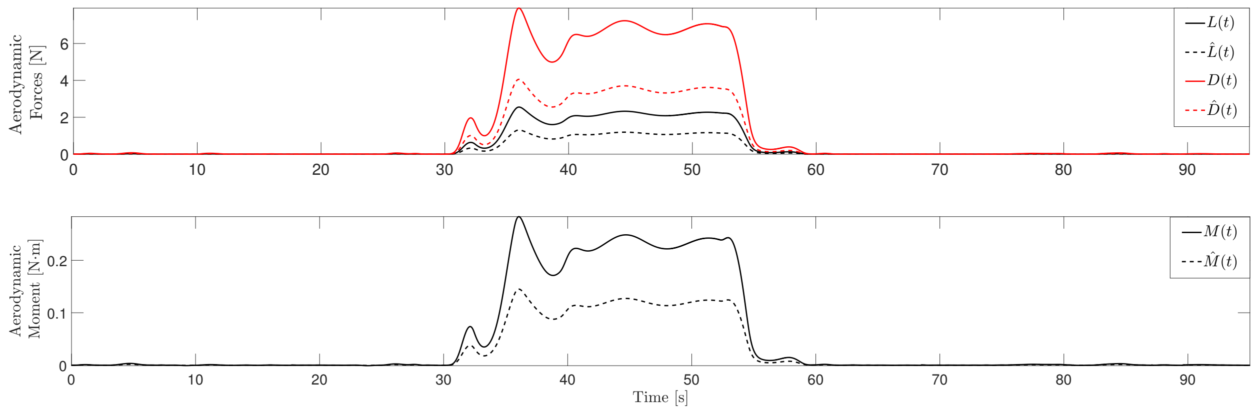

Fig. 16 Aerodynamic lift, drag, moment of the aerodynamic forces acting on the quad-biplane following the trajectory shown in Figure 12 , and their estimates. Over the time intervals $[0, 30]$s and $[50, 95]$s, the quad-biplane is commanded to hover, and hence, the aerodynamic forces and moment are small. Over the time interval $(30, 50)$s, the quad-biplane is commanded to fly forward, and hence, the aerodynamic forces and moment are large. Remarkably, the aerodynamic lift contributes to following the desired reference altitude.

[42] Fantoni, I., and Lozano, R., *Non-linear Control for Underactuated Mechanical Systems*, Springer, Berlin, Germany, 2002.

[43] Carter, G. I., and Eagen, S., "Autonomous Quad Biplane UAV with Adaptive Control Law – Preliminary Flight Test Results," https://youtu.be/XXTcToseCFw, 2021. Last accessed 11/17/2021.